

Improved Synthesis and Thermal Stability of Electrode-supported α -alumina Separator
for Lithium Ion Batteries

by

Gaurav Sharma

A Thesis Presented in Partial Fulfillment
of the Requirements for the Degree
Master of Science

Approved June 2016 by the
Graduate Supervisory Committee:

Jerry Y.S. Lin, Chair
Candace Chan
Arunachala Kannan

ARIZONA STATE UNIVERSITY

August 2016

ABSTRACT

Lithium ion batteries have emerged as the most popular energy storage system, but they pose safety issues under extreme temperatures or in the event of a thermal runaway. Lithium ion batteries with inorganic separators offer the advantage of safer operation. An inorganic separator for lithium ion battery was prepared by an improved method of blade coating α -Al₂O₃ slurry directly on the electrode followed by drying. The improved separator preparation involves a twice-coating process instead of coating the slurry all at once in order to obtain a thin (~40 μ m) and uniform coat. It was also found that α -Al₂O₃ powder with particle size greater than the pore size in the electrode is preferable for obtaining a separator with 40 μ m thickness and consistent cell performance. Unlike state-of-the-art polyolefin separators such as polypropylene (PP) which are selectively wettable with only certain electrolytes, the excellent electrolyte solvent wettability of α -Al₂O₃ allows the coated alumina separator to function with different electrolytes. The coated α -Al₂O₃ separator has a much higher resistance to temperature effects than its polyolefin counterparts, retaining its dimensional integrity at temperatures as high as 200°C. This eliminates the possibility of a short circuit during thermal runaway. Lithium ion batteries assembled as half-cells and full cells with coated α -Al₂O₃ separator exhibit electrochemical performance comparable with that of polyolefin separators at room temperature. However, the cells with coated alumina separator shows better cycling performance under extreme temperatures in the temperature range of -30°C to 60°C. Therefore, the coated α -Al₂O₃ separator is very promising for application in safe lithium-ion batteries.

Dedicated to my parents,

Alka and Rajpal Sharma

and my sister,

Meenal Sharma

You are my strength and the reason I could dream to do this.

ACKNOWLEDGMENTS

Firstly, I would like to express my deepest gratitude to my parents for being my pillars of support. Your sacrifices and belief in me are the reasons I could embark on this journey. Your love and encouragement drove me every single day to keep working hard. Thank you for making the right decisions for me as I grew up, and in the process enabled me to make the right decisions for myself.

I would like to thank my advisor, Dr. Jerry Y.S. Lin for his incredible mentorship and guidance. In spite of me not having any background in lithium ion batteries, you believed in my abilities. With the help of your constant motivation, I got the confidence to expand my limits. Your deep involvement in my projects was very beneficial and was crucial in maintaining the pace of work. I learnt several life lessons from you like leadership, punctuality, accountability, dedication and hard work to name a few. As an engineer and aspiring scientist, I thank you for steering my life and career path in the right direction.

I would like to thank Dr. Arunachala Kannan and Dr. Candace Chan for their willingness to serve on my committee. Their expertise and knowledge helped this project at a fundamental level which I have applied throughout my research. I appreciate their recommendations and valuable feedback. I would also like to thank Fred Pena for promptly helping in fixing equipment issues in the lab. Without his help, a lot of valuable research time would have been lost.

Lastly, I would like to thank all the current and former members of Dr. Lin's group from whom I learnt a great deal. It was an absolute pleasure to work alongside

such a talented group of people: Dr. Linghui Yu, Dr. Xueliang Dong, Dr. Wanliang Mi, Dr. Alexandra Kasik, Dr. Xiaoli Ma, Dr. Zebao Rui, Dr. Lie Meng, Dr. Sainan Liu, Dr. Yang Liu, Dr. Hong Meng, Dr. Xuefei Sun, Dr. Nick Linneen, Dr. Margarita Judith Ramirez, Han-Chun Wu, Joshua James, Suzanne Williams, Fateme Benihashemi, Amr Ibrahim, Jiansong Miao, Narayan Kanhere, Chris Bremer and Paul McAfee.

I would like to thank China Electric Power Research Institute (CEPRI) for their financial support to this project. I would also like to thank Celgard and Entek for providing PP and PE polymer separators for this research respectively.

TABLE OF CONTENTS

	Page
LIST OF TABLES	viii
LIST OF FIGURES	ix
CHAPTER	
1 INTRODUCTION	1
1.1 Overview	1
1.2 Statement of the Problem.....	2
1.3 Approach.....	3
1.4 Objectives of Research and Thesis Structure.....	5
2 IMPROVED SYNTHESIS AND THERMAL STABILITY OF COATED ALUMINA SEPARATOR	7
2.1 Introduction	7
2.2 Experiment	8
2.2.1 Preparation and Characterization of Coated Ceramic Separator.....	8
2.2.2 Cell Assembly	9
2.2.3 Electrochemical Characterization.....	10
2.3 Results and Discussion	11
2.3 Conclusions	26
3 EFFECT OF ALUMINA POWDER PARTICLE SIZE ON CELL PERFORMANCE.....	27
3.1 Introduction	27
3.2 Effect of Alumina Powder Particle Size on Slurry Quality	32
3.3 Effect of Alumina Powder Particle Size on Coating Quality	36

CHAPTER	Page
3.4 Effect of Small and Large Particle Size Alumina Powders on Cell	
Performance	38
3.4.1 Preparation of Coated Ceramic Separator	38
3.4.2 Cell Assembly.....	39
3.4.3 Electrochemical Characterization	39
3.5 Results and Discussion.....	39
3.6 Conclusions	42
4 HIGH TEMPERATURE STUDY ON NMC/LTO FULL CELL	44
4.1 Introduction.....	44
4.2 Experiment	48
4.2.1 Preparation of Separator	48
4.2.1 Cell Assembly.....	48
4.2.3 Electrochemical Characterization.....	49
4.3 Results and Discussion	50
4.4 Conclusions	55
5 SUMMARY AND RECOMMENDATIONS.....	56
5.1 Summary.....	56
5.2 Recommendations	58
REFERENCES	59
APPENDIX	
A PROCEDURES TO ASSEMBLE HALF-CELLS AND FULL-CELLS	62
B CYCLE TESTING OF CELLS	65

APPENDIX	Page
C ELECTROCHEMICAL IMPEDANCE SPECTROSCOPY OF CELLS	67
D PROCEDURE TO MEASURE POROSITY OF COATED ALUMINA SEPARATOR	69
E DETERMINATION OF OHMIC RESISTANCE OF SEPARATOR USING EIS	71

LIST OF TABLES

Table	Page
2.1. Fitted Impedance Parameters of LTO/Li Cells with PP and Coated-Alumina Separator.	18
3.1. Grades of α -Alumina Formed into Slurry in the wt. ratio 1:0.8 (α -Alumina: 5wt% PVA Soln.) Different Amounts of DI Water is Added Depending on the Powder to Obtain Desired Consistency of Slurry.....	33

LIST OF FIGURES

Figure		Page
2.1.	Schematic Diagram of the Cross-Section of a Typical LTO/Li Half-Cell with Coated Alumina Separator	9
2.2.	Comparison Between Once- And Twice- Coated α -Al ₂ O ₃ Separator of 40 μ m Thickness. (A) LTO Electrode with α -Al ₂ O ₃ Separator Coated Once (Left) and Coated Twice (Right). (B) Charge-Discharge Curves of Cells with Once- and Twice-Coated α -Al ₂ O ₃ Separators.	12
2.3.	SEM Images of 40 μ m Thick α -Al ₂ O ₃ Separator Coated on LTO Electrode (A) Surface, (B) Particles and (C) Cross-Section	13
2.4.	EDS Analysis of a 75 μ m Thick Al ₂ O ₃ Separator Coated on LTO: (A) Element Spectrum, (B) SEM Image of Cross-Section and (C) Element Mapping on the Cross-Section Filtered for Aluminum (Red) and Titanium (Green).....	14
2.5.	(A) Conductivity of Different Electrolytes in Coated α -Al ₂ O ₃ and PP Separator. (B) Charge-Discharge Cycling of Cell with Coated α -Al ₂ O ₃ Separator Soaked with Electrolyte B	16
2.6.	Charge-Discharge Curves of LTO/Li Cells with 40 μ m and 100 μ m Thick Coated Alumina Separator and PP Separator Cycled at 0.2C Rate.	17

Figure	Page
2.7. Nyquist Impedance Plots of LTO/Li Cells with PP and 40 μm Thick Coated Alumina Separator. Equivalent Circuit Shown Inset	18
2.8. Charge-Discharge Curves of a Half-Cell at 0.2C Rate in which the NMC Cathode is Coated with 60 μm Thick Alumina Separator and Li Foil is the Anode	19
2.9. Rate Capability of LTO/Li Cells with 40 μm Thick Coated Alumina Separator and PP Separator at Room Temperature	20
2.10. Long-Term Cycling Stability Test for LTO/Li Cells with 40 μm Thick Coated Alumina Separator and PP Separator at 0.2C	21
2.11. Shrinkage of Coated-Alumina, PE and PP Separators with Respect to Increasing Temperature	22
2.12. Coated-Alumina, PP and PE Separators at (A)-(C) Room Temperature and (D)-(F) 180°C Respectively	23
2.13. Performance of LTO/Li Cells at 0.5 C-Rate with Coated-Alumina and PP Separator at Different Temperatures	24
3.1. Resistance Vs Thickness Plots of Celgard PP2500 and A15SG Separators	30
3.2. Slurry of A10325 Grade Alumina Powder Coated on LTO Electrode with 50 μm Blade Gap.	37

Figure	Page
3.3. Slurry of A14325 Grade Alumina Powder Coated on LTO Electrode with 50 μm Blade Gap.	37
3.4. Charge-Discharge Curves for LTO/Li Half Cells with 40 μm Thick AKP30 Separator at 0.2C Rate.	40
3.5. SEM Image of Lithium Titanium Oxide (LTO) Electrode at 10000x (Left) and 2500x (Right)	41
3.6. Charge-Discharge Curves of Three LTO/Li Half Cells with 40 μm Thick A17SG Separator at 0.2C Rate.	42
4.1. Charge-Discharge Curve of a Full Cell with NMC Cathode Coated with 60 μm Thick Alumina Separator. A Bare Piece of LTO is the Anode. The Cell was Cycled at 0.3 mA.	51
4.2. Charge-Discharge Curve of a Full Cell with LTO Anode Coated with 60 μm Thick Alumina Separator. A Bare Piece of NMC is the Cathode. The Cell Was Cycled at 0.3 mA.	51
4.3. Charge-Discharge Curve of a Full Cell with NMC Cathode and LTO Anode. The Separator Used is the Celgard PP2500 (Polypropylene). The Cell was Cycled at 0.3 mA.	52

Figure	Page
4.4. Charge-Discharge Curve of a Full Cell with NMC Cathode and LTO Anode. The Separator Used is the Entek Teklon Gold LP (Polyethylene). The Cell was Cycled at 0.3 mA.	53
4.5. Cell Impedance as a Function of Increasing Temperature Measured for NMC/LTO Full Cells with Coated-Alumina, PE and PP Separators at 1 KHz Galvanostatic EIS Frequency.....	54

CHAPTER 1

INTRODUCTION

1.1 Overview

The emergence of lithium-ion batteries (LIB) as the most popular energy storage system is mainly due to their high energy density, no memory effect, low self-discharge and long cycle life. They find application in a wide variety of portable electronic devices as well as electric vehicles and smart grids. [1, 2] A LIB is a secondary cell which consists of three major components, the anode (negative electrode), the cathode (positive electrode) and the electrolyte. The electrodes in a LIB are intercalation materials that allow the lithium ions to get inserted into their crystal structures. Some common cathode materials are Lithium Cobalt Oxide (LCO), Lithium Iron Phosphate (LFP) and Lithium Manganese Oxide (LMO) among others. Lithium Nickel Manganese Cobalt Oxide (NMC) cathode is a new generation of cathode material that is preferred for its high specific energy and low self-heating rate. On the other hand, Graphite is the most commonly used anode material, but newer materials like Lithium Titanium Oxide (LTO) are also becoming attractive due to their “zero-strain” property.

The electrolyte in a LIB is usually a non-aqueous solution of organic solvents. Since LIBs operate at a voltage higher than the voltage at which electrolysis of water occurs (1.23 V), it is not possible to use aqueous electrolytes. Hence, organic solvents such as Ethylene Carbonate (EC), Diethyl Carbonate (DEC), Dimethyl Carbonate (DMC), Propylene Carbonate (PC) etc. are mixed in different combinations with varying volume ratios depending upon the application and desired property. These organic solvents are stable in the voltage range of LIBs but are still not conductive of lithium

ions. Lithium salts such as Lithium hexafluorophosphate (LiPF_6) and Lithium bis(oxolato)borate (LiBOB) are added to the organic solvents to form a stable electrolyte that conducts lithium ions.

Since the need of the hour is to have compact LIBs for high energy density and low internal resistance, the electrodes have to be stacked with minimal distance between them. Since the electrolyte is liquid, the electrodes would touch each other and the cell would short circuit. Hence, a separator is used to overcome this issue.

The separator has a few basic functions. It must be an electronically insulating material so that no short circuit can occur. It must be porous and be wettable by the non-aqueous electrolytes. This is essential so that the separator can soak up the ion conducting electrolyte. The separator must be thin so that the ohmic resistance is not large. Also, the separator must be chemically inert in the cell environment.

1.2 Statement of the problem

There have been relatively frequent occurrences of battery fires and explosions, which are a major cause of concern. [3] A significant source of this flammability, along with the electrolyte, is the polymeric separator used widely in commercial lithium-ion batteries. [4] They are generally polyolefins with low melting points, poor mechanical strength and are combustible. In case of overcharging or thermal runaway, the elevated temperatures ($>100^\circ\text{C}$) can cause them to shrink, melt and finally, short the electrodes. [5, 6]

Since most lithium-ion battery systems continue to be based on liquid electrolytes, it is essential that separators are wettable by a wide range of commercial as well as novel electrolytes. However, commercial polyolefin separators like polyethylene (PE) and

polypropylene (PP) have an intrinsic hydrophobic surface character and low surface energy. This results in poor electrolyte wettability and retention which affects the cycle life of the battery. The slow wetting of the separator causes a bottleneck in battery manufacturing, increasing production time. [7]

1.3 Approach

Inorganic materials have been studied as a solution to the limitations of polyolefin separators. [8] Their high hydrophilicity and surface area render them excellent wettability with essentially all non-aqueous electrolytes. Not only that, they also exhibit exceptional mechanical stability over a wide temperature range because of their ceramic nature. [5]

A popular approach to introduce inorganic separator in lithium ion batteries is to coat a layer of inorganic powder mixed with a binder on the surface of polyolefin separators. Alumina (Al_2O_3) is one of the preferred ceramic powders for this purpose due to its low cost. [9] Shi et al. [10] blade coated one side of the PE separator with a layer of nano-sized Al_2O_3 powder mixed with a carboxymethyl cellulose (CMC) and styrenebutadiene rubber (SBR) mix binder. Similarly, Choi et al. [11] dip coated both the sides of the PE separator with nano-sized Al_2O_3 powder mixed with Poly(lithium 4-styrenesulfonate) binder. These separators show enhanced wettability and dimensional stability at high temperatures ($>100^\circ\text{C}$), but the thickness of the coating layers is just 3-9 μm . This means that the bulk of the separator is still polymeric in nature and will combust in the event of a thermal runaway.

To overcome this problem, efforts have been directed towards synthesizing inorganic separators with minimum polymer content. Zhang et al. [12,13] pressed CaCO_3

powder with Teflon binder to form free standing separators. Wang and co-workers sintered Al_2O_3 and SiO_2 powders to obtain free standing separators. [14,15] The common issue with these free standing separators was that their brittle nature would require them to be very thick ($\sim 200\mu\text{m}$). This large thickness would increase the cell's internal resistance and decrease energy density. Their brittleness makes them difficult to handle in a large scale manufacturing setup. Also, sintering is a highly energy intensive process that would escalate the cost of the separator.

To reduce the thickness of inorganic separators, Chen et al. [16] used a $60\mu\text{m}$ thick anodic alumina membrane as a separator. Wang and co-workers [17] synthesized a $\sim 50\mu\text{m}$ thick flexible mesh of alumina nanowires using hydrothermal treatment method. From a cost and ease manufacturing standpoint, the synthesis procedure of both of these separators is complex and chemically intensive. On the other hand, thin free standing separators have been synthesized that avoid the sintering process, but for that they have to contain a large amount of polymeric binder. Raja et al. [18] prepared a $30\text{-}50\mu\text{m}$ thick MgAl_2O_4 separator with 30 wt% PVdF-HFP binder while Holtmann et al. [19] synthesized a $22\mu\text{m}$ thick Boehmite separator with 25 wt% PVdF binder. In the event of a battery fire, the organic binder part would combust and severely damage the separator.

A new approach to obtain thin inorganic separators was reported by Kim et al. [20] which involved directly dip-coating graphite anode sheets into a slurry of alumina powder, PVdF-HFP binder and acetone followed by drying. The cells prepared showed good cycling performance and improved thermal stability. Industrial fabrication of lithium ion batteries includes blade-coating of cathode and anode on metal sheet from their respective slurry. [21] Recently, Lin and coworkers [22] reported a blade-coated

alumina separator on LTO anode using inexpensive commercial alumina powder. This separator coating method uses an alumina slurry rather than a suspension, which minimizes the drying required. More importantly, the separator coating method can be scaled up easily and incorporated into existing battery fabrication process.

1.4 Objectives of research and thesis structure

Lin and co-workers [22] demonstrated that lithium ion battery with such a 100 μm thick alumina coated separator has comparable electrochemical performance as the same battery with 25 μm thick commercial polypropylene separator. Even though in that work they reported the coating of a 40 μm thick alumina separator on the anode by the blade coating method, the separator layer of such thickness was not of good integrity so good performance of the lithium ion battery with the thin alumina separator could not be obtained.

The objective of this research is to report the coating of a thin (40 μm) alumina separator by an improved blade coating method and excellent electrolyte wettability of the thin alumina separator. Several standard cell performance tests were also conducted like charge-discharge cycling, rate capability, long-term cycling and electrochemical impedance spectroscopy to show the comparable performance of cells with coated alumina separator and commercial PP separator at room temperature. However, this work also shows that lithium ion batteries with the thin alumina separator have better cell thermal stability and electrochemical performance under extreme temperature conditions than those with polymer separator. The study then takes a closer look at the effect of alumina powder particle size used for preparing the separator on the cell performance. And finally, the coated alumina separator is used in a NMC/LTO full cell and tested for

the improvement in battery safety in the event of a thermal runaway in which the internal temperature of a cell can rise greatly.

CHAPTER 2

IMPROVED SYNTHESIS AND THERMAL STABILITY OF COATED ALUMINA SEPARATOR

2.1 Introduction

As discussed in Chapter 1, Mi et al. [22] had established the feasibility of the approach of coating a slurry of alumina powder on the LTO electrode as a separator for LIBs. Their work was successful in demonstrating the chemical and mechanical stability of the separator in the cell environment by conducting cycling tests and XRD analysis. They also showed the improved dimensional stability of the separator with increasing temperature compared to the commercial PP separator. However, the synthesis procedure reported by them was only able to yield a thick separator of $\sim 100\ \mu\text{m}$ thickness and they reported their results for the same.

A thick separator is not preferable because it is bulky and will increase the weight of the cell. This reduces the energy density of the battery. Also, a thick separator will directly affect the ohmic resistance of the cell as it increases the distance between the electrodes. This affects the power capability of the cell as the increased internal resistance makes it difficult to operate the battery at higher C-rates. This section of the study focuses on improving the synthesis procedure of the coated alumina separator in order to obtain a thickness as low as $\sim 40\ \mu\text{m}$. The electrochemical performance of this thin separator is reported along with its thermal stability. The inherent quality of excellent wettability of alumina with different types of electrolytes is also explored as a significant advantage over commercial polymer separators. The study then extends into demonstrating the improved cell performance under extreme temperatures.

2.2 Experiment

2.2.1 Preparation and characterization of coated ceramic separator

The thin porous α -Al₂O₃ separator was coated directly on lithium titanium oxide (Li₄Ti₅O₁₂) and lithium nickel manganese cobalt oxide (LiNi_{1/3}Mn_{1/3}Co_{1/3}O₂) (NMC) electrodes (CEPRI, Beijing, China) by a two-step blade coating process. The electrodes were made up of micron sized LTO and NMC particles (BTR, China), carbon black (Timcal, Switzerland) and polyvinylidene fluoride (PVdF) (HSV900, Arkema, France) in the weight ratios of 90:5:5. The LTO electrode active material had been coated, dried and pressed down to a thickness of 80 μ m on 20 μ m thick aluminum foils and NMC electrode active material had a thickness of 65 μ m on 25 μ m thick aluminum foil. The active material loading on the LTO electrode was 90 g m⁻² and for NMC electrode it was 83 g m⁻².

For the preparation of the separator, a commercially available α -Al₂O₃ powder (A17SG) (Alcoa Inc., Pittsburgh, PA) was mixed with 5 wt% polyvinyl alcohol (PVA) solution (average molecular weight of 77000-79000) (ICN Biomedicals, Inc.) and deionized water. Their weight ratio was maintained at 1.0:0.8:2.4 respectively. A homogenous slurry was obtained after stirring the mixture for 15 minutes. The first coating step involves setting a blade gap of 25 μ m on a caliper-adjustable doctor blade (Digital II Micrometer Film Applicator) (Gardco LLC, Pompano Beach, FL) to spread the first layer of the slurry on the electrode. The electrode had been taped down on a flat glass surface. The coated electrode was then dried in a humidity-controlled chamber which maintains the temperature at 40°C and 60% relative humidity for 8 h. Next, the second and final coat of the slurry was applied by setting the blade gap to 50 μ m. This

was followed by the same humidity-controlled drying process as in the first step. The coated electrode was then cut into 16 mm diameter disks using a disk cutter (Compact & Precision Disc Cutter with Standard 16 mm Diameter Cutting Die, MSK-T-10) (MTI, Richmond, CA). The cut disks were subjected to vacuum drying for 6 h at 60°C to obtain a final separator layer thickness of 40 μm . The alumina-coated electrodes were ready for cell assembly.

The morphology of the prepared separator was observed using scanning electron microscope (SEM, Philips FEI XL-30) after gold deposition. The porosity of the separator was measured based on the geometric dimensions, weight and density ($\rho_{\text{alumina}} = 3.95 \text{ kg m}^{-3}$) of the coated layer. To evaluate separator shrinkage with increasing temperature, a 45x45 mm piece of LTO coated with 40 μm thick alumina separator layer was compared to commercial polypropylene (PP2500) (Celgard LLC, Charlotte, NC) and polyethylene separators (Teklon Gold LP) (ENTEK, Lebanon, OR) of the same dimensions placed on top of LTO pieces. The three separators were then heated simultaneously in a high temperature oven (MTI, Richmond, CA).

2.2.2 Cell assembly

All the cells assembled in this work were CR2032 type coin cells (X2 Labwares, Singapore). For the half-cells, the LTO or NMC electrode were the cathode while 0.1 mm thick lithium metal chips (MTI, Richmond, CA) were used as the anode. A commercial electrolyte was used which was a solution of 1 M LiPF_6 in equal volume of ethyl carbonate (EC), diethyl carbonate (DEC) and dimethyl carbonate (DMC) (EC:DEC:DMC = 1:1:1, v/v/v) (MTI, Richmond, CA) in most experiments. A second electrolyte was prepared by adding 0.5 M LiBOB salt (Sigma-Aldrich) to propylene

carbonate (PC) (anhydrous 99.7%, Sigma-Aldrich) and shaking well. The solution was then kept at 80° C for 24 h until all the salt dissolved. The coin cells were assembled in an argon-filled glove box (Innovative Technology Inc, Amesbury, MA), in which oxygen and moisture content were kept below 0.5 ppm.

A typical half-cell was assembled by placing a 16 mm diameter alumina-coated LTO or NMC disk into the CR2032 casing. The separator was then filled with 150 μ L of the electrolyte and then covered with a 14 mm diameter lithium metal chip. Spacers and spring completed the cell which was then sealed using a coin cell crimper (MSK-110) (MTI, Richmond, CA) with a pressure of 400 psi. Depending on electrode, each cell contained about 14.9 mg of LTO or 15 mg of NMC active material. Similarly, half-cells with PP separator were also prepared using LTO as cathode and lithium metal chip as anode for comparison. A schematic of a typical cell is shown in Figure 2.1.

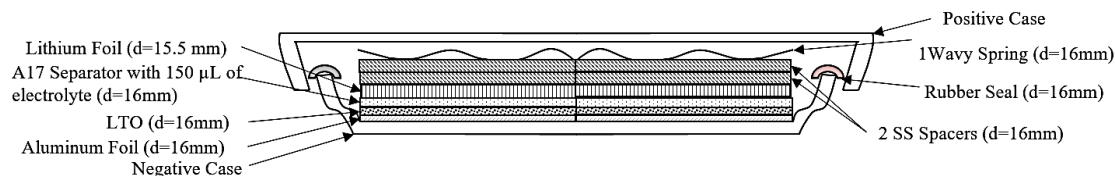


Figure 2.1 Schematic diagram of the cross-section of a typical LTO/Li half-cell with coated alumina separator.

2.2.3 Electrochemical characterization

The charge-discharge cycling characteristics of the cells was tested using NEWARE battery testing system (BTS3000) (Neware Co, Shenzhen, China). The cut-off voltage window setting for LTO half cells was 1.0-2.5 V, for the NMC half cells it was 3.0-4.4 V and for the NMC/LTO full cells it was 0.5-3.5 V. All the cells were cycled using the CC-CV (Constant Current – Constant Voltage) charging regime. The C-rates in

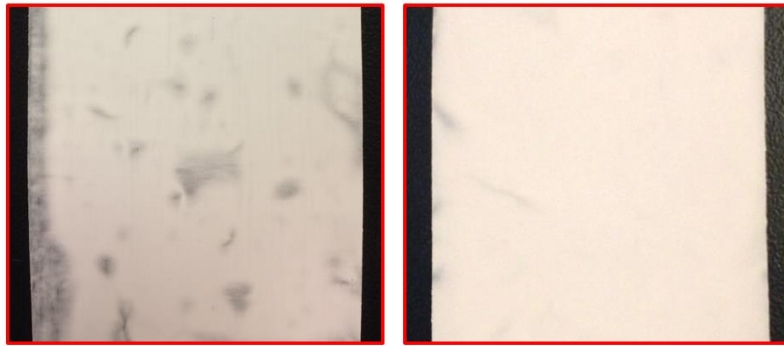
the rate capability test were calculated based on 2.6 mAh capacity of the LTO electrode. To test the cell performance under extreme temperature conditions, the cells were inserted into a low temperature oven (temperature range: -40 to 150 °C) (WD4005, Shanghai Jianheng Instruments, Shanghai, China). The conductivity of the electrolytes in the different separators was measured by soaking the separators in the electrolyte for 24 h. The soaked separator was inserted between two stainless steel plates. The ohmic resistance was then obtained by using PARSTAT 2263 EIS station (Princeton Applied Research, Oak Ridge, TN). In the case of coated alumina separator, the separator coating was kept supported on a thin aluminum foil for this test. The scanning parameters were set to a starting frequency of 100 kHz, end frequency of 100 mHz and an AC amplitude of 10 mV rms. Nyquist plots for the fully charged cells (100% SOC) was also obtained using the same EIS parameters, except for the end frequency which was set to 10 mHz.

2.3 Results and Discussion

The one-step coating method reported by Mi et al. [22] can only produce a uniform and continuous separator having a thickness greater than 50 μm . When attempts were made to lower the thickness by reducing the blade gap, the slurry would tend to slide off the smooth electrode surface due to the large shear force from the blade. It was hypothesized that the lack of sufficient frictional force on the electrode surface to counter the shear force from the blade prevents the retention of slurry. Based on this understanding, a two-step coating method was conceptualized in which the first coat of alumina powder was intended to make the electrode surface rough.

High quality 40 μm thick separator can be coated on the LTO or NMC electrode by the following two-step coating method. An electrode is placed on an ethanol-wetted

glass surface. After applying the alumina slurry on the electrode surface, a caliper-adjustable doctor blade with gap set at 25 μm is drawn over the electrode so as to obtain a discontinuous deposition of the alumina slurry. The purpose of this coat is to make the electrode surface rough for the second coat. The electrode is then dried in humid conditions. For the second and final coat, the dried coated electrode is again laid flat on the glass surface followed by application of more alumina slurry. This time, the blade gap is set at 50 μm and the doctor blade is drawn over the electrode. The quality of the coat is now uniform with continuous coverage of the electrode surface with the slurry as seen in the right hand side image of Figure 2.2 (a). This is because the roughness from the first coat induces frictional forces to oppose the shear forces from the doctor blade. This retards the slurry from sliding away over the electrode surface, resulting in greater slurry retention and a uniform coat.



(a)

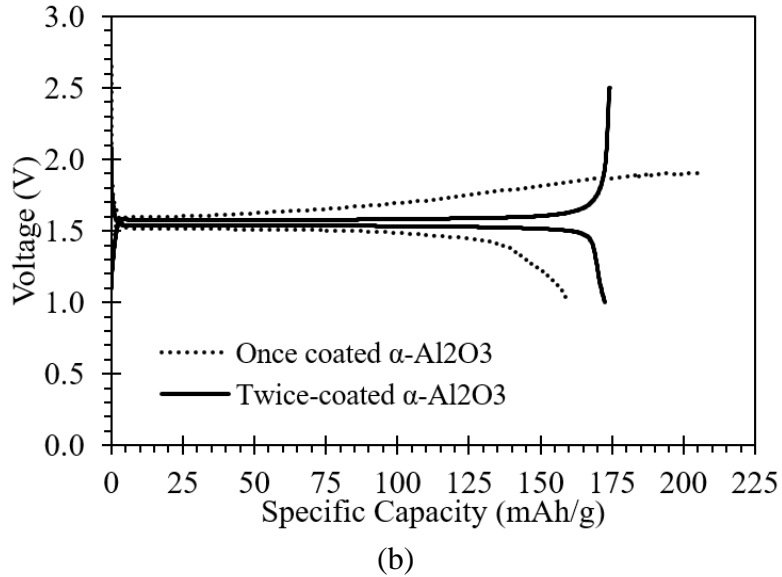


Figure 2.2. Comparison between once- and twice- coated α -Al₂O₃ separator of 40 μ m thickness. (a) LTO electrode with α -Al₂O₃ separator coated once (left) and coated twice (right). (b) Charge-discharge curves of cells with once- and twice-coated α -Al₂O₃ separators.

Attempting to coat the separator in one step directly with a 50 μ m blade gap results in a patchy and irregular coat as seen in the left hand side image of Figure 2.2 (a). This is because the slurry tends to slide off the smooth electrode surface. When assembled into a cell, these uncoated areas allow the electrodes to come in contact with each other and the cell short circuits as seen in Figure 2.2 (b). On the other hand, the cell with the twice-coated 40 μ m thick separator is able to successfully charge and discharge. The SEM images in Figure 2.3 confirm the crack-free nature of the separator.

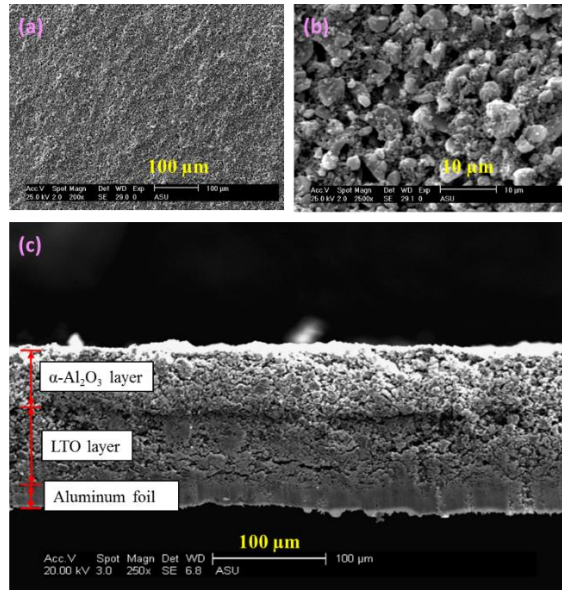


Figure 2.3. SEM images of 40 μm thick $\alpha\text{-Al}_2\text{O}_3$ separator coated on LTO electrode (a) surface, (b) particles and (c) cross-section

Figure 2.4 provides an insight into the elemental compositions and distribution using EDS scans. A 75 μm thick coated alumina separator was analyzed over its cross section as shown in Figure 2.4 (b). Also, Figure 2.4 (a) shows the elemental spectrum obtained. Carbon (C) comes from the binders present in the separator as well as the electrode. Aluminum (Al) is present in the separator as Al_2O_3 and in the bottom foil as pure Al. The electrode contains titanium (Ti). The sample was sputter coated with Au/Pd. The cross section was then mapped for Al and Ti to confirm the layered structure as shown in Figure 2.4 (c). The top Al_2O_3 separator layer and bottommost pure-Al foil layer are mapped in red for Al, whereas the LTO layer glows up in green for the Ti (light element Li was undetectable by the EDS). The red patches in the green LTO layer are stray Al_2O_3 particles. These few loose particles are pushed down while cutting the sample and spread over the cross section. The EDS scans help us distinguish between the layers and make the interfaces more apparent.

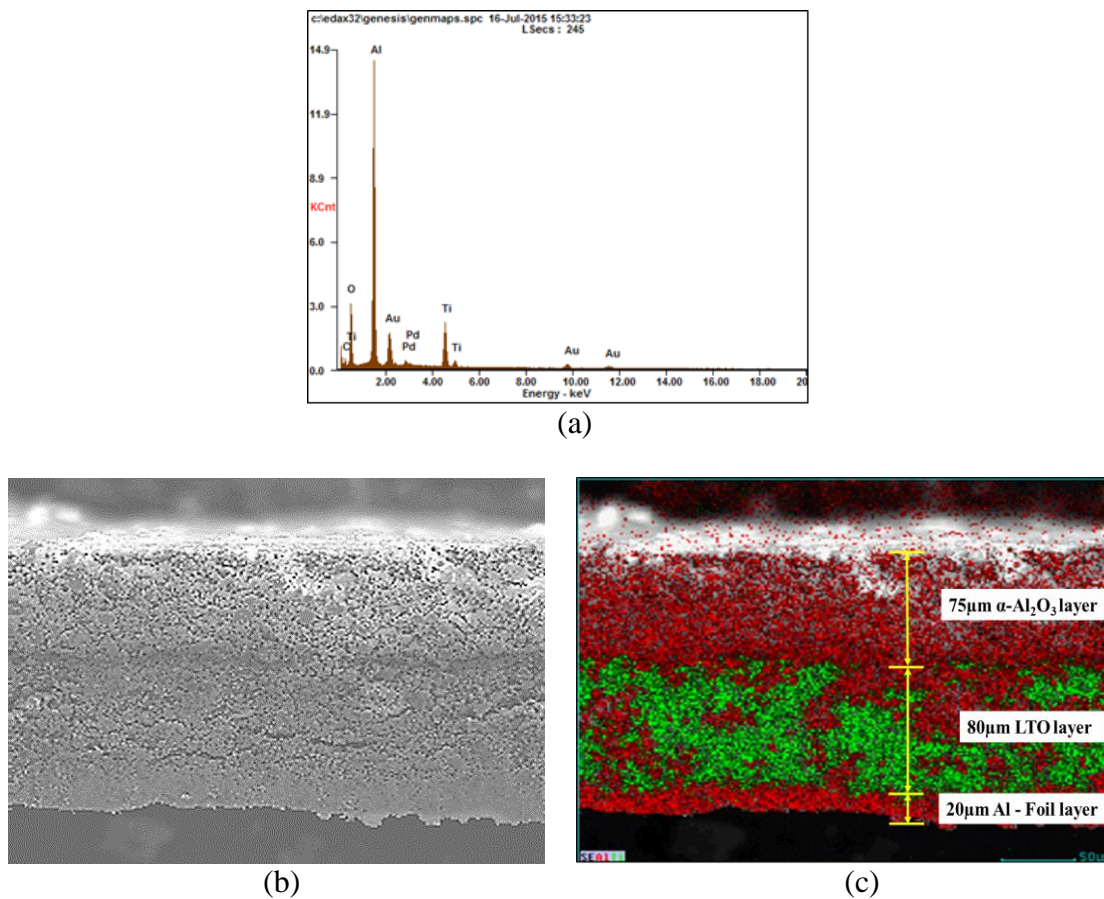
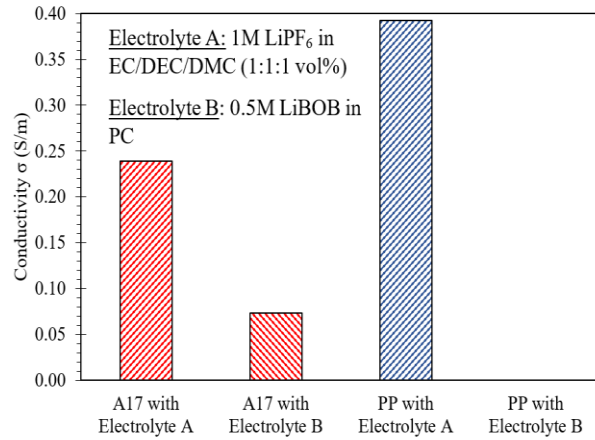


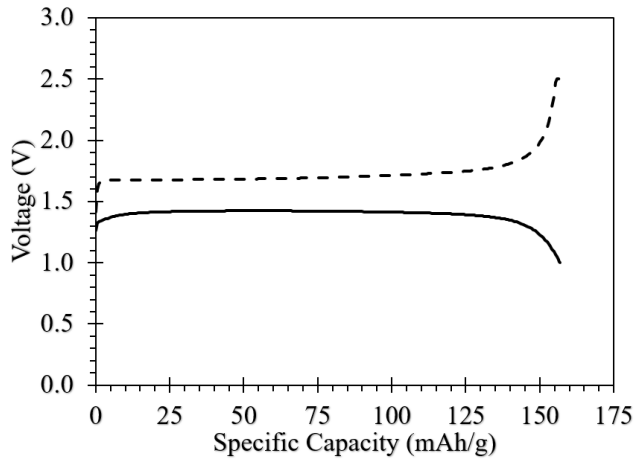
Figure 2.4. EDS analysis of a 75µm thick Al₂O₃ separator coated on LTO: (a) Element Spectrum, (b) SEM image of cross-section and (c) Element mapping on the cross-section filtered for Aluminum (Red) and Titanium (Green)

To examine the wettability of the electrolyte with the separator, coated α -Al₂O₃ separator and PP separator were soaked in two different electrolytes and the conductivity was measured. Electrolyte A was a commercial 1 M LiPF₆ in EC/DEC/DMC (1:1:1 vol%) electrolyte and Electrolyte B was 0.5M LiBOB in PC. These electrolytes were chosen because of the high dielectric constants of EC and PC solvents, which makes them difficult to be soaked by the hydrophobic polyolefin separators like PP. [24] Figure 2.5 (a) shows that the coated α -Al₂O₃ separator is able to soak both the electrolytes and

allows lithium ions to conduct, whereas PP separator is unable to get wet by Electrolyte B. As a result, a cell with coated α -Al₂O₃ separator and Electrolyte B can cycle successfully as shown in Figure 2.5 (b). Due to the lower ionic conductivity of Electrolyte B, the voltage gap is wider. This is a major advantage of the inorganic separators as they are compatible with not just the commercial electrolytes, but also the novel and specialized electrolytes that continue to be developed.



(a)



(b)

Figure 2.5. (a) Conductivity of different electrolytes in coated α -Al₂O₃ and PP separator. (b) Charge-discharge cycling of cell with coated α -Al₂O₃ separator soaked with Electrolyte B.

The effects of successfully reducing the thickness of the coated alumina separator from 100 μm (as reported by Mi et al. [22]) to 40 μm can be seen in the charge-discharge characteristics of the cells. LTO/Li cells with 40 μm and 100 μm thick coated alumina separator as well as PP separator were cycled at 0.2C rate using CC-CV charging. In Figure 2.6, we can observe the reduction in the voltage gap between the charge and discharge curves of the cell with 40 μm alumina separator as compared to the cell with 100 μm alumina separator. This can be attributed to the lower ohmic resistance due to a thinner separator. Also, a thicker separator will contain a greater amount of binder than a thinner one on absolute weight basis. A higher amount of binder in the separator increases the charge transfer resistance to the active material interface in the cell [22], which also contributes to the overall increase in the cell internal resistance. On the other hand, the charge-discharge curves of the cells with 40 μm coated alumina separator and PP separator are closer to each other, showing the comparable electrochemical performance of the two separators.

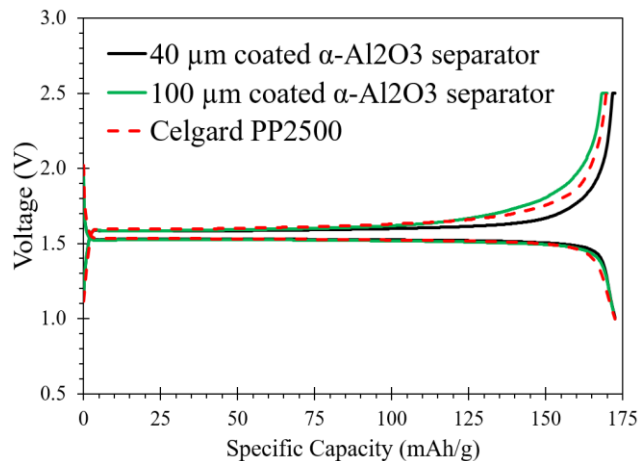


Figure 2.6. Charge-discharge curves of LTO/Li cells with 40 μm and 100 μm thick coated alumina separator and PP separator cycled at 0.2C rate.

Figure 2.7 shows the Nyquist plots for the two LTO/Li cells with the coated 40 μm $\alpha\text{-Al}_2\text{O}_3$ separator and PP separator soaked in the commercial electrolyte [1 M LiPF_6 in EC/DEC/DMC (1:1:1 vol%)]. The impedance parameters were obtained after fitting the data to the equivalent circuit (shown inset) using EC-Lab software. The impedance parameters are listed in Table 2.1 along with the thickness and porosity of the separators. The parameter R_1 represents the ohmic resistance in the cell due to the electrolyte in the separator. R_2 represents the charge transfer resistance at the interface of the active material particles. As expected, the R_1 value of cell with PP separator (2.86 Ω) is lesser than that of the one with coated $\alpha\text{-Al}_2\text{O}_3$ separator (5.72 Ω) since it is a thinner and more porous separator. The R_2 values of the coated $\alpha\text{-Al}_2\text{O}_3$ separator (262.13 Ω) and PP separator (279.36 Ω) are also quite similar to each other which explains their comparable performance.

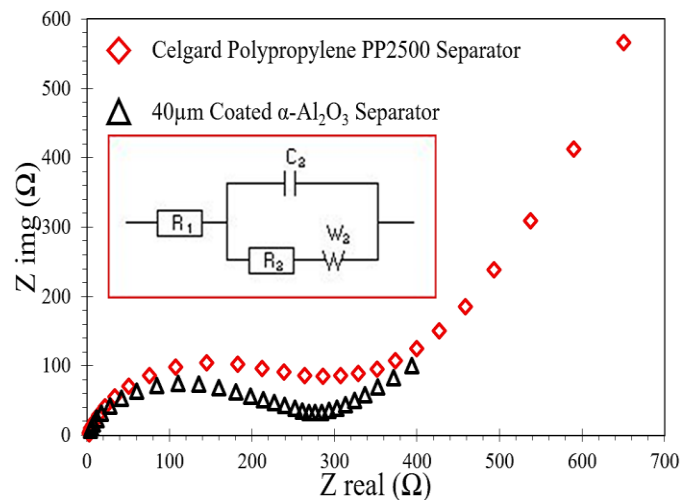


Figure 2.7. Nyquist impedance plots of LTO/Li cells with PP and 40 μm thick coated alumina separator. Equivalent circuit shown inset.

Table 2.1. Fitted impedance parameters of LTO/Li cells with PP and coated-alumina separator.

Separator	Thickness (μm)	Porosity (%)	R₁ (Ω)	R₂ (Ω)
Celgard PP2500	25*	55*	2.86	279.36
Coated $\alpha\text{-Al}_2\text{O}_3$	40	48.68	5.72	262.13

* Data from manufacturer Celgard LLC

To investigate the versatility in applying this coated alumina separator to other lithium-ion battery electrodes, we coated the NMC cathode with a 60 μm thick $\alpha\text{-Al}_2\text{O}_3$ separator using the one-step blade coating procedure outlined by Mi et al. [22] The coating obtained was uniform and yielded good quality separators which were later assembled into half-cells with lithium foil and tested at 0.2C rate. Figure 2.8 shows the successful charging-discharging of the coated-NMC half-cell. This indicates that the alumina separator can be coated on both anodes and cathodes. In this study, LTO was chosen over NMC as the electrode to be coated with $\alpha\text{-Al}_2\text{O}_3$ separator because it is a zero-strain electrode [29] as well as for experimental consistency. A dimensionally stable electrode will act as a good substrate for this separator since it is directly supported by the electrode.

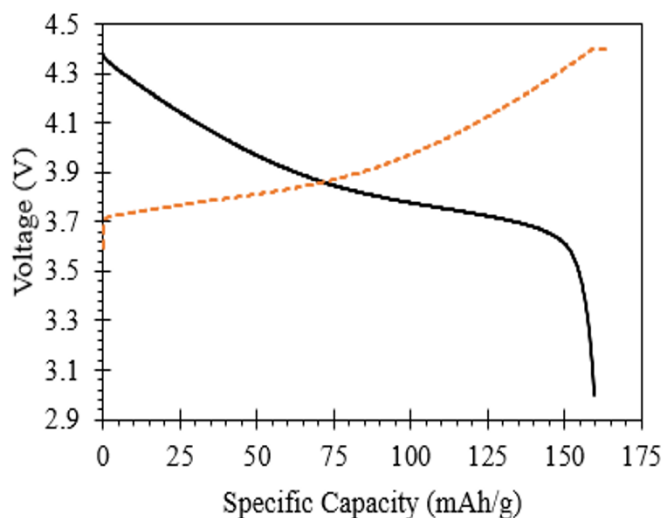


Figure 2.8. Charge-discharge curves of a half-cell at 0.2C rate in which the NMC cathode is coated with 60 μm thick alumina separator and Li foil is the anode.

Figure 2.9 shows the ability of the coated $\alpha\text{-Al}_2\text{O}_3$ separator to function at different C-rates. Two LTO/Li cells were assembled, one with 40 μm thick coated $\alpha\text{-Al}_2\text{O}_3$ separator and the other with PP separator. Initially, the cells underwent formation cycles at 0.1C rate. The cell with alumina separator attained steady state faster than the cell with PP separator owing to the better wettability of the alumina separator. The C-rate was then increased to 0.2C, 0.5C, 1C, 2C, 4C and back to 0.2C after 10 cycles at each C-rate. As expected, the capacity of the cells decrease with increasing C-rate due to increasing overpotential. The performance of the two cells is similar up to 2C rate. Only at a very high C-rate of 4C does the cell with coated-alumina separator cease to cycle as the potential drop due to the ohmic overpotential becomes significant.

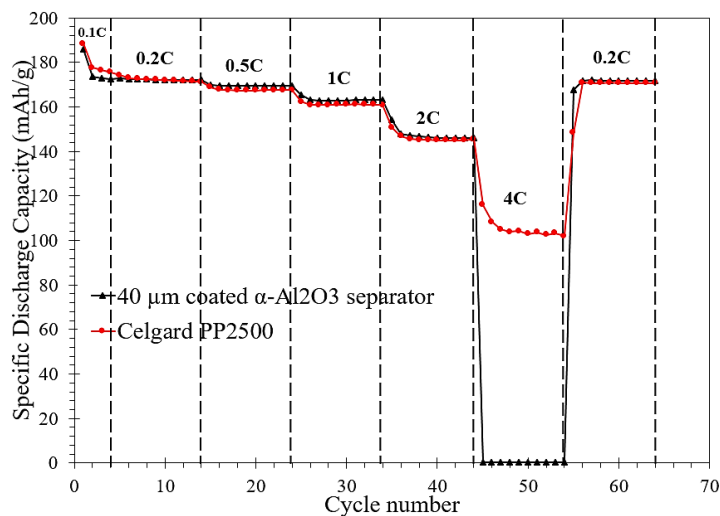


Figure 2.9. Rate capability of LTO/Li cells with 40 μm thick coated alumina separator and PP separator at room temperature.

A good separator must possess chemical inertness and mechanical integrity within a cell environment. This is important from the viewpoint of long-term cell cycling performance. To study this, the coated-alumina and PP separators were tested for 100 cycles at 0.2C rate in LTO/Li half-cells. Capacity in each cycle was measured and capacity retention percentage, defined as specific discharge capacity in a given cycle to that in the first cycle, is plotted versus cycle number in Figure 2.10. We can see that even after 100 cycles, both the cells are able to retain more than 98% of their initial capacities. The minor fluctuations in the capacity can be associated with electrolyte degradation over such a long duration of cycling in a pure lithium anode half-cell.

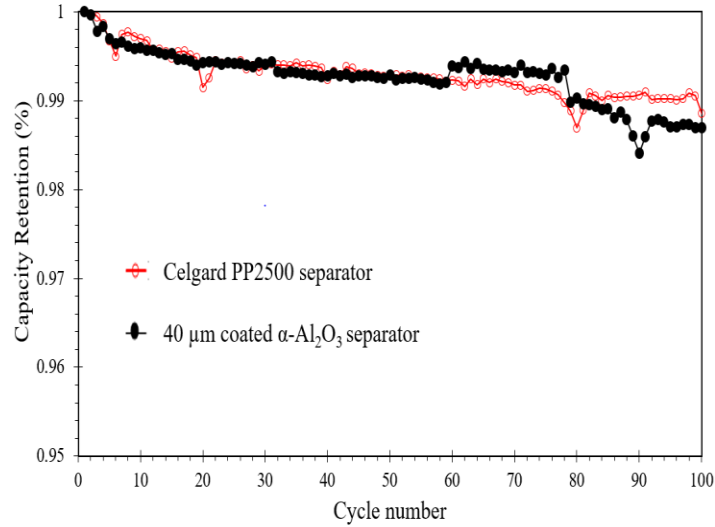


Figure 2.10. Long-term cycling stability test for LTO/Li cells with 40 μm thick coated alumina separator and PP separator at 0.2C

Thermal runaway in a battery is dependent on separator shrinkage and melting. [25] Rising cell temperatures can cause the polymeric separators to shrink and eventually melt, resulting the contact of electrodes and short-circuiting the cell. This phenomenon can be quantified by exposing the separators to increasing temperatures in a stepwise manner and observing the shrinkage. This approach has been found to be representative of the battery safety characteristics. [30] For this study, the coated-alumina separator, PP and PE separators were compared. The initial area of the separator samples at room temperature was recorded as S_0 . Then, at every temperature step the area of the separators was measured and recorded as S_t . The shrinkage percent, calculated by $(S_0 - S_t)/S_0$, is plotted versus temperature in Figure 2.11.

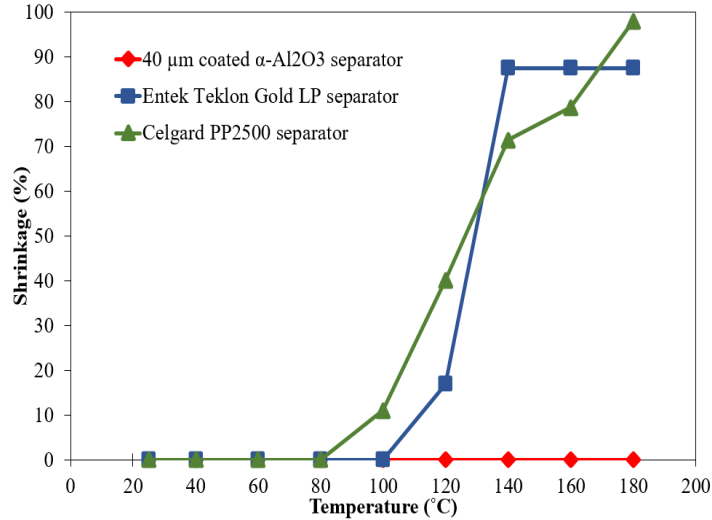


Figure 2.11. Shrinkage of coated-alumina, PE and PP separators with respect to increasing temperature.

From the shrinkage data shown in Figure 10, the PP and PE separators shrink significantly above 80°C and 100°C respectively. The PE separator melted completely at around 130°C whereas the PP separator melted at around 160°C. The coated-alumina separator did not show any dimensional change at any point in the entire temperature range owing to the excellent thermal stability of inorganic materials. The initial (25°C) and final state (180°C) of the separators was photographically recorded to show the extent of shrinkage and melting as seen in Figure 2.12. The PP separator curls until it melts, whereas the PE separator shrinks equally on all of its edges before melting. No shrinkage for the coated-alumina separator.

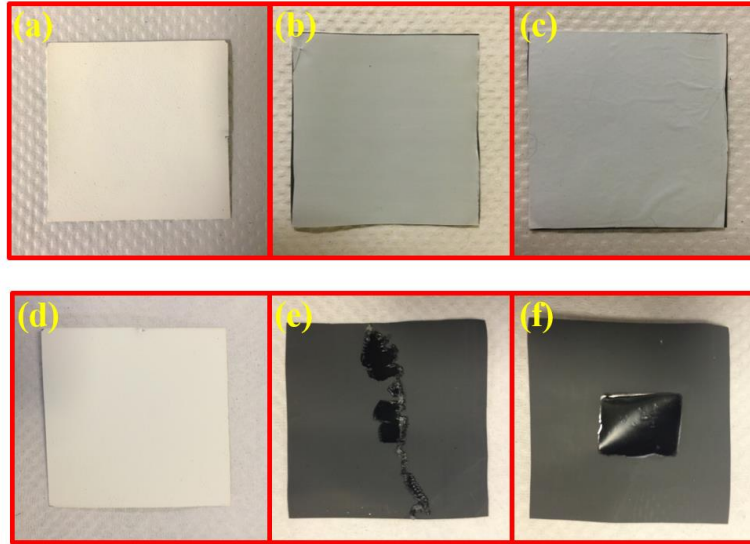


Figure 2.12. Coated-alumina, PP and PE separators at (a)-(c) room temperature and (d)-(f) 180 °C respectively.

Lithium-ion battery performance is affected by fluctuating ambient temperatures which may arise due to weather changes or inefficient battery pack temperature management systems. [26] To emulate these possible extremities in ambient conditions, LTO/Li half cells with PP and coated α -Al₂O₃ separator were placed in a low temperature chamber. While the cell cycling performance was being recorded, the temperature inside the chamber was first decreased stepwise from 25°C to -30°C. The cells were allowed to cycle five times at every temperature step. Then, the temperature was increased from -30°C to 60°C in the same stepwise sequence. The capacity retention for both the cells was plotted against the cycle number in Figure 2.13. As the temperature is reduced, the conductivity of the electrolyte decreases which further increases the ohmic polarization. [27] The larger voltage drop in the cell with coated-alumina separator causes the cell to reach cut-off voltage quicker than the cell with PP separator. This explains the greater capacity loss for coated-alumina cell compared to PP cell till -10°C. However, at

extremely low temperatures of -20°C and -30°C , the lithium-ion diffusivity is severely slowed down. This is where the inherent characteristics of the $\alpha\text{-Al}_2\text{O}_3$ powder prove to be advantageous as reported by Liao et al. [28]

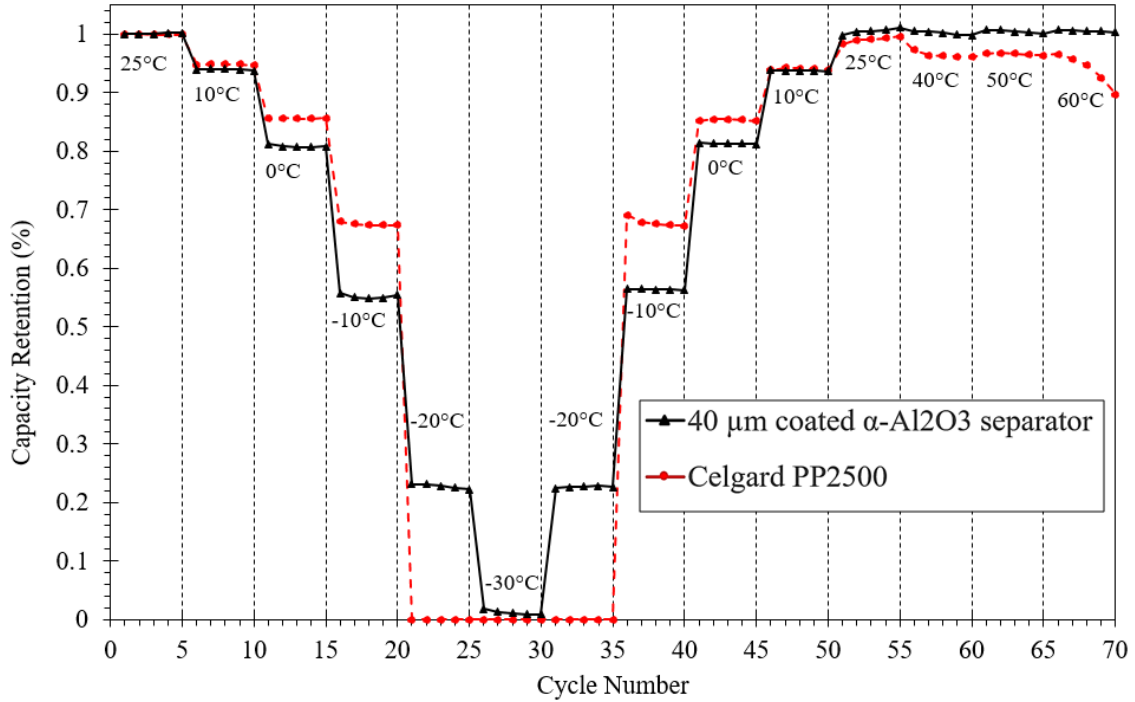


Figure 2.13. Performance of LTO/Li cells at 0.5 C-rate with coated-alumina and PP separator at different temperatures.

The excellent electrolyte solvent wettability of the $\alpha\text{-Al}_2\text{O}_3$ particles allows the coated-alumina separator to retain the electrolyte more effectively due to the larger capillary forces as compared to PP separator. This facilitates lithium-ion conduction in the coated-alumina separator filled with the liquid electrolyte even below -20°C whereas the cell with PP separator cannot. Both the cells recovered their capacities when temperature is increased back to 25°C . Upon further increasing the temperature to 40°C , 50°C and 60°C , the capacity begins to fade rapidly in the cell with PP separator while the cell with coated-alumina separator maintains its capacity. This is because at high

temperatures, thermal decomposition of LiPF_6 salt occurs in which it reacts with the trace amount of moisture present in the electrolyte.



This highly reactive HF causes deterioration of the electrode active material and corrodes the solid-electrolyte interface (SEI) layer, thus reducing the capacity as seen in case of cell with PP separator. [31] However, alumina has been known to have a scavenging effect on HF which prevents electrode degradation and capacity fade. [32] Hence, there are benefits of using alumina separator under extreme temperatures.

2.4 Conclusions

The two-step blade coating procedure has made it possible to obtain continuous and good quality electrode-supported $\alpha\text{-Al}_2\text{O}_3$ separator of 40 μm thickness. The excellent electrolyte solvent wettability of $\alpha\text{-Al}_2\text{O}_3$ even with highly hydrophobic solvents makes it compatible with a wide range of electrolytes. The simplicity of the technology allows for coating of the $\alpha\text{-Al}_2\text{O}_3$ separator on various electrodes. At room temperature, the electrochemical performance of the cell with the coated $\alpha\text{-Al}_2\text{O}_3$ separator is comparable to that of cells with commercial PP separator. However, at high temperatures the mechanical and dimensional stability of the coated alumina separator is far superior to that of commercial polymer separators. This is advantageous in preventing battery short circuiting during thermal runaway that arises due to separator shrinkage or melting. Even under cold and hot ambient temperature conditions, cells with the coated $\alpha\text{-Al}_2\text{O}_3$ separator exhibits better cycling performance and lower capacity fade than cells with PP separator.

CHAPTER 3

EFFECT OF ALUMINA POWDER PARTICLE SIZE ON CELL PERFORMANCE

3.1 Introduction

In chapter 2, the synthesis of coated alumina separator prepared from A17SG grade alumina powder had been optimized. But a closer look needs to be taken at the effect of alumina powder quality and particle size on cell performance and to understand why A17SG gave good results.

Inorganic materials have received great attention in recent years for application in energy storage devices, mainly on the separator. The two most widely reported inorganic materials are alumina (Al_2O_3) and silica (SiO_2) due to their low cost. Inorganic materials have high hydrophilicity which makes them easily wettable by most LIB electrolytes. They exhibit exceptional chemical, mechanical and thermal stability in a battery environment. They are also reported to have scavenging abilities and help reduce the degrading effect of moisture and other impurities in LIBs. As a result of having so many advantages, inorganic materials are increasingly being incorporated into LIB separators, either as an additive or coating on existing polymer separators, or as pure inorganic separators.

Most inorganic separators reported so far make use of the inorganic materials in their powder form mainly for two reasons. Firstly, it is easier to process inorganic materials in their powder form. Secondly, hydrophilicity is a surface phenomenon, therefore using inorganic materials in their powder form results in better utilization of this property as powders have high surface area. The effect of this improved wettability

can be observed in the MacMullin number determination of coated alumina separator when compared to that of commercial polymer separator like Celgard PP2500.

The MacMullin number is a widely accepted parameter in the battery separator community and extensive research has already been done on it. The ratio of the resistivity of a separator membrane to that of the electrolyte is called the MacMullin number, N_m . It describes the relative contribution of a separator to cell resistance. It factors out the thickness of the material and assumes that the separator wets completely in the electrolyte used for the test.

The equation to calculate N_m is as follows:

$$N_m = \frac{\text{Resistivity of separator filled with electrolyte } (\rho_s)}{\text{Resistivity of electrolyte } (\rho_e)} = \frac{\Omega_s \times A \times \sigma_e}{t}$$

Where:

Ω_s is the ohmic resistance of the separator filled with electrolyte (Ohms)

σ_e is the conductivity of the pure electrolyte (S/m)

A is the cross-sectional area of the separator (m^2)

t is the thickness of the separator (m)

Abraham et al. [42] suggested another relationship between the MacMullin number and porosity by introducing a tortuosity parameter, τ , i.e.,

$$N_m = \frac{\tau^2}{\varepsilon}$$

The experiment to determine the MacMullin number is fairly simple [42-48] and uses the same setup as the conductivity test as described earlier in Chapter 2. The steps to determine the MacMullin number of Celgard PP2500 and coated alumina separator (A15SG grade in this case) was as follows:

1. Soak at least 3 pieces of 19 mm diameter PP separator for 24 hours in the 1M LiPF₆ in EC/DEC/DMC (1:1:1 v/v/v) electrolyte.
2. Polish and press two identical stainless steel disks of 16 mm diameter to make them very flat and smooth. When held against each other, there should be no visible space in between them.
3. Measure the resistance of these disks using EIS between 100 kHz and 100 mHz frequency. This is recorded as Ω_{ss} . It should be ensured that they are well aligned when held against each other.
4. The soaked PP separators are then placed in between the disks one by one. Extra electrolyte is added to ensure good wettability. The ohmic resistance is measured after every layer is added. This is recorded as Ω_{sep+ss} .
5. The difference between Ω_{sep+ss} and Ω_{ss} is the ohmic resistance of the PP separator.
6. The experiment was performed in the same way for coated-alumina separator. The only difference is that the alumina slurry is coated on pure aluminum foil. Because of this, the blank reading is obtained with the aluminum foil placed in the between the stainless steel disks.

The resistance values obtained for both PP and A15SG are plotted against their thickness as shown in Figure 3.1. After line fitting, the slope is used to calculate MacMullin number as shown below:

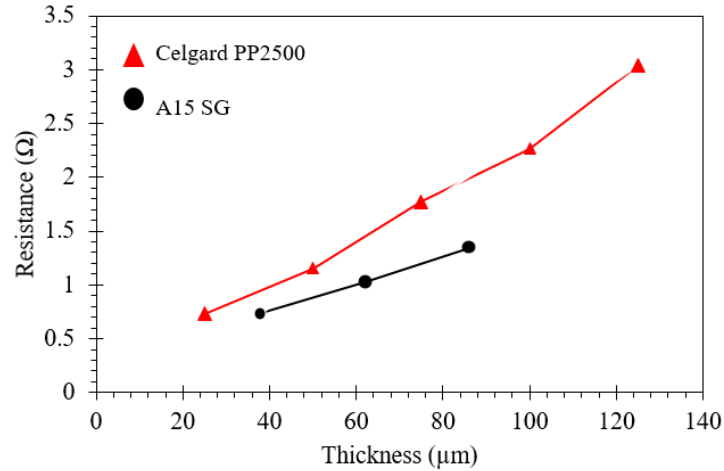


Figure 3.1: Resistance vs Thickness plots of Celgard PP2500 and A15SG separators

Resistance/ μm = slope

For PP = $0.0229 \text{ } \Omega/\mu\text{m}$

And for A15 SG = $0.0127 \text{ } \Omega/\mu\text{m}$

Therefore,

$$\text{PP2500: } Nm = 0.0229 \times \pi \times (8000)^2 \times 1.1 \times 10^{-6}$$

$$Nm = 5.064$$

$$\text{A15SG : } Nm = 0.0127 \times \pi \times (8000)^2 \times 1.1 \times 10^{-6}$$

$$Nm = 2.809$$

Porosity: The porosity for PP is provided by the supplier (55%). For A15SG, the porosity is measured using geometric dimensions and weight, which was found to be 66.64%. This is a very high porosity. Usually, when a porous electrode is coated with alumina slurry, the capillary forces cause the slurry to shrink as it dries, resulting in a lower porosity. Hence, the coated alumina separator prepared on Al foil is not comparable to the coated alumina separator formed on LTO or NMC electrode. But this

data is useful for understanding the advantage of particulate morphology and good wettability for inorganic powders.

Tortuosity: the tortuosity of the two separators can be calculated using the following relation:

$$\tau = (\varepsilon * Nm)^{0.5}$$

$$\text{Celgard PP2500} : \tau = (0.55 * 5.07)^{0.5} = 1.67$$

$$\text{A15 SG} : \tau = (0.6664 * 2.809)^{0.5} = 1.37$$

As we can see, the MacMullin number for A15SG is lower than that of PP. This indicates that for a given thickness, the A15 SG inorganic separator would provide lower cell internal resistance than PP. This is likely due to higher porosity, lower tortuosity and better wettability. This can explain why coated inorganic separator with higher thickness (40 μm) are still able to give comparable charge-discharge curves as that of the thinner (25 μm) Celgard PP2500 separator.

In spite of several advantages of using inorganic material powders in separators, not a lot of research efforts have been made towards understanding the role of powder particle size in determining the cell performance. Takemura et al. [40] prepared free standing inorganic separators by preparing slurry of alumina powder, poly (vinylidene fluoride) (PVdF) binder and *N*-methyl-2-pyrrolidone (NMP) as the solvent. The slurry was blade coated on a glass surface and the NMP solvent was allowed to dry. The film was then peeled off to obtain a free standing separator of 20 μm thickness. The ratio of powder to binder was varied. Also, two different particle sized alumina powders were studied, one with 0.01 μm and the other with 0.3 μm . Separator with 0.01 μm particle

size were found to be more suitable due to their better electrolyte retention in the pores due to higher capillary force as well as their lower Gurley values.

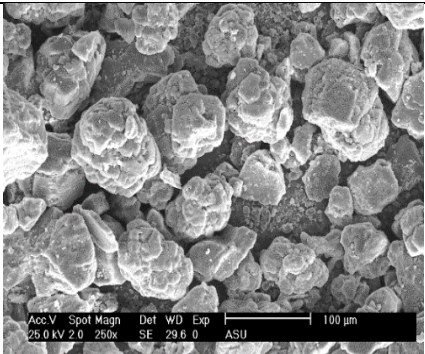
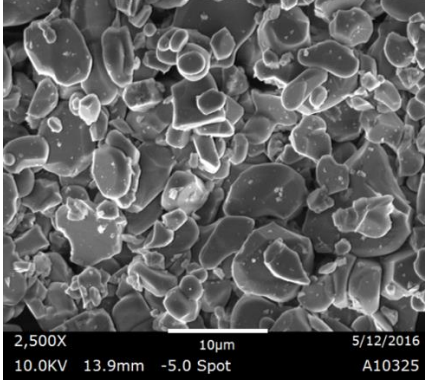
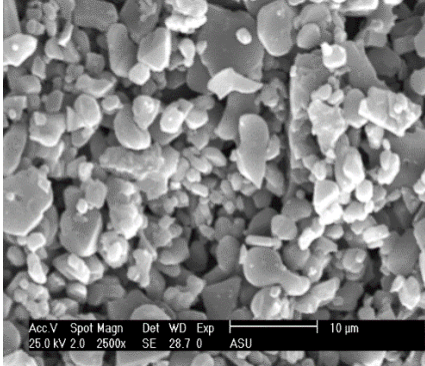
The results reported by Takemura and co-workers are interesting but are not applicable in the case of coated alumina separator since theirs is a free standing separator. In the case of coated alumina separator, the slurry of alumina particles is applied directly on the electrode. Hence, the electrode is not isolated from the fabrication of separator and the slurry can affect the electrode properties directly. The aim of this chapter is to take a closer look at how the alumina powder particles size affects the slurry consistency, quality of coating obtained on the electrode and finally, the electrochemical performance.

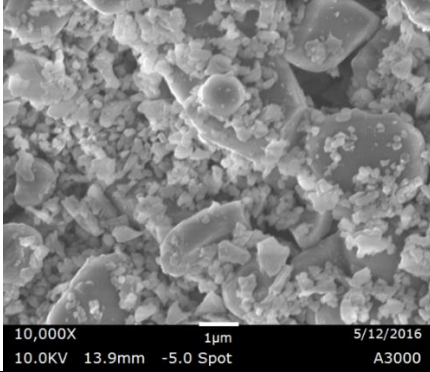
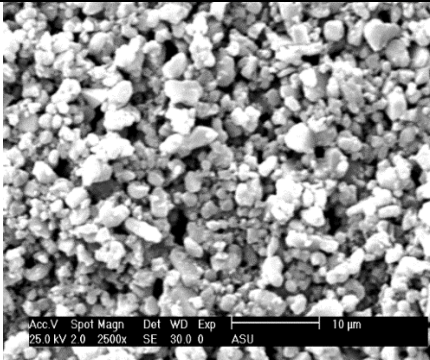
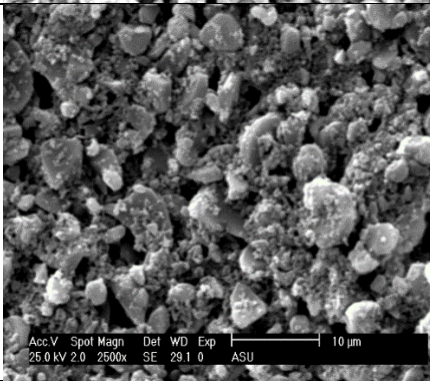
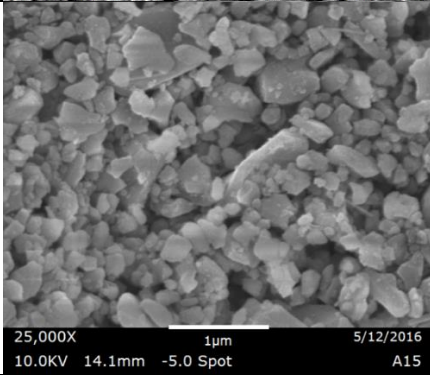
3.2 Effect of alumina powder particle size on slurry quality

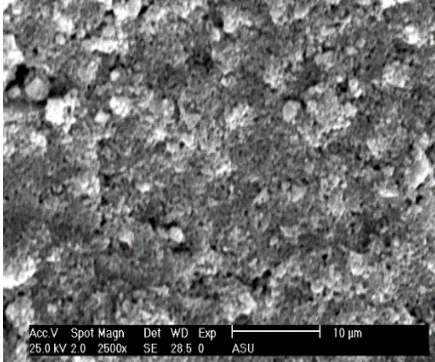
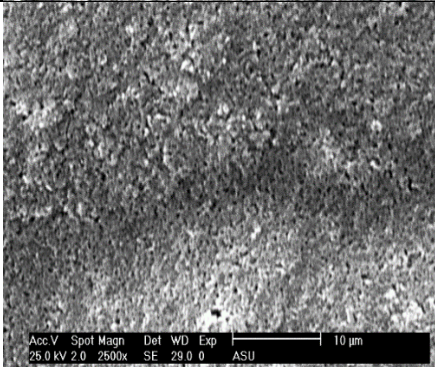
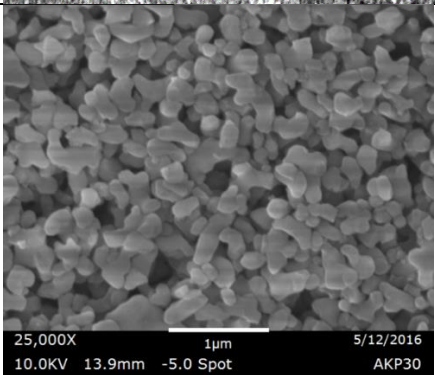
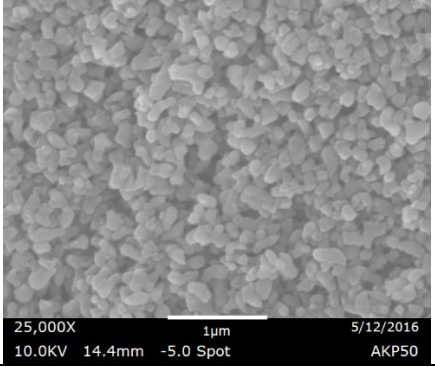
The coated-alumina separator for Lithium-ion batteries is obtained by coating a slurry of alumina powder on the electrode (anode or cathode). The slurry is prepared by mixing α -alumina powder, and 5wt% PVA soln. in the ratio 1:0.8 by weight. DI water is added to this mix and stirred thoroughly until a fairly thick and uniform slurry with no powder aggregates is obtained. This slurry is then spread over a flat electrode and coated using a two-step coating process to obtain a separator layer of 40 μm thickness with 0.4wt% PVA by weight after drying.

To obtain this separator, it is very important to obtain a uniform slurry easily. There should be no sedimentation, aggregation or froth formation of the powder. The alumina powder used has some effect on the quality of the slurry obtained. Table 3.1 summarizes all the different grades of α -alumina available in our lab and describes their slurry quality.

Table 3.1: Grades of α -alumina formed into slurry in the wt. ratio 1:0.8 (α -alumina: 5wt% PVA soln.) Different amounts of DI water is added depending on the powder to obtain desired consistency of slurry.

Grade	Supplier	SEM	Particle size (μm)	Slurry quality (0.4 wt% PVA and DI water)
A13	Alcoa		50-100	Particles too large and heavy to be able to disperse in water 
A10325	Alcoa		5-15	
A14325	Alcoa		1-10	

A3000	Alcoa		0.2-6	
A2750	Alcoa		1-5	
A17SG	Alcoa		0.1-5	
A15	Alcoa		0.1-0.5	

A15SG	Alcoa		0.5	
A16SG	Almatis		0.4	High degree of aggregation retained along with froth formation in the slurry. 
AKP-30	Sumitomo		0.27	
AKP-50	Sumitomo		0.2	

Almost all grades of alumina are able to form uniform slurries except for A13 and A16SG. In case of A13, the particle size is very large because of which the particles tend

to settle down. For A16SG, the aggregates in the powder are small. They are difficult to break down by just the stirring motion in the beaker.

Therefore, the following conclusions can be drawn about the effect of alumina powder particle size and quality on slurry consistency:

1. Alumina particle size should be $< 20 \mu\text{m}$. Large particles are heavy and the slurry experiences sedimentation.
2. If the particle size is $< 1 \mu\text{m}$, then care must be taken that there are no aggregates in the powder. These aggregates are very difficult to break down while stirring the slurry. If there are any aggregates in the powder, an extra ball-milling step will be required before the slurry can be prepared.
3. Powders with particle size between $1 \mu\text{m}$ and $20 \mu\text{m}$ also contain aggregates, but these aggregates are large and weak. They are easily broken down by the stirring motion of the glass rod in the beaker. Hence, uniform slurry is obtained without requiring any ball-milling.

3.3 Effect of alumina powder particle size on coating quality

It is essential that the alumina powder is able to produce $40 \mu\text{m}$ thick alumina separator of good quality. All the powders that were able to form a slurry of desired consistency were then coated on LTO electrodes using the two-step blade coating procedure described in Chapter 2. Among these powders, A10325 and A14325 were the only two powders that were unable to coat the electrode as seen in Figure 3.2 and Figure 3.3 respectively.

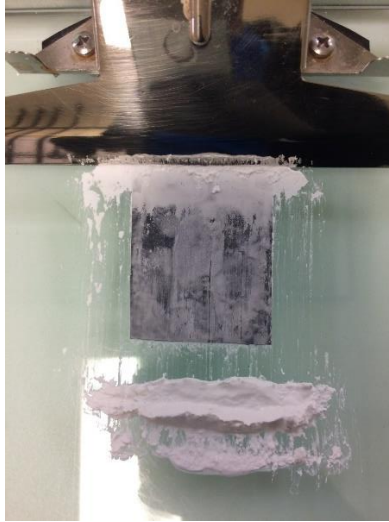


Figure 3.2. Slurry of A10325 grade alumina powder coated on LTO electrode with 50 μm blade gap.



Figure 3.3. Slurry of A14325 grade alumina powder coated on LTO with 50 μm blade gap.

As seen in Figure 3.2 and Figure 3.3, the slurry could not coat the LTO electrode. It appears as though the slurry was pushed away by the doctor blade. This must be because the particle size ($\sim 15 \mu\text{m}$) is very large compared to the blade gap itself (50 μm). Therefore, the slurry experiences a large shear force and cannot adhere to the electrode surface.

Hence, this study helps in further narrowing down the particle size range of alumina powder for preparing coated alumina separator. From these observations, it can be approximated that alumina powders with particle sizes $<10\ \mu\text{m}$ are more likely to form a good consistency slurry as well as a good quality $40\ \mu\text{m}$ separator on the electrode.

3.4 Effect of small and large particle size alumina powders on cell performance

From a slurry preparation and coating quality point of view, the previous two studies lead to the conclusion that any alumina powders with particle size less than $10\ \mu\text{m}$ and no aggregates can produce good quality separator. However, this still leaves a large particle size range from nanometer size to $10\ \mu\text{m}$. Also, it is not clear what is the effect of these particle sizes on cell performance.

Therefore, two powders were selected to study the effect of alumina particle size on cell performance. The first powder was AKP30, which has an average particle size of $270\ \text{nm}$. The second powder was A17SG which has an average particle size of $\sim 5\ \mu\text{m}$ with a small fraction of nano-sized particles.

3.4.1 Preparation of coated ceramic separator

The thin porous $\alpha\text{-Al}_2\text{O}_3$ separator was coated directly on lithium titanium oxide ($\text{Li}_4\text{Ti}_5\text{O}_{12}$) electrodes by the two-step blade coating process as described in Chapter 2.

For the preparation of the A17SG separator (Alcoa Inc., Pittsburgh, PA), the powder was mixed with 5 wt% polyvinyl alcohol (PVA) solution (average molecular weight of 77000-79000) (ICN Biomedicals, Inc.) and deionized water. Their weight ratio was maintained at 1.0:0.8:2.4 respectively. In case of AKP30 separator (Sumitomo Chemicals, Tokyo), the only change was made in the weight ratio which was 1.0:0.8:3.8

respectively. The morphology of the bare LTO electrode was observed using scanning electron microscope (SEM, Amray 1910) after gold deposition.

3.4.2 Cell assembly

CR2032 type coin cells were assembled (X2 Labwares, Singapore). The cells were half-cells with LTO as cathode while 0.1 mm thick lithium metal chips (MTI, Richmond, CA) were used as the anode. A commercial electrolyte was used which was a solution of 1 M LiPF₆ in equal volume of ethyl carbonate (EC), diethyl carbonate (DEC) and dimethyl carbonate (DMC) (EC:DEC:DMC = 1:1:1, v/v/v) (MTI, Richmond, CA). The cell was assembled in the same fashion as described in Chapter 2.

3.4.3 Electrochemical characterization

The charge-discharge cycling characteristics of the cells was tested using NEWARE battery testing system (BTS3000) (Neware Co, Shenzhen, China). The cut-off voltage window setting for the LTO half cells was 1.0-2.5 V. All the cells were cycled using the CC-CV (Constant Current – Constant Voltage) charging regime.

3.5 Results and Discussion

Four LTO/Li half-cells with AKP30 grade alumina separator coated on the LTO electrode were cycled at 0.2C-rate. All the four cells were assembled in identical conditions with the same materials. In spite of making sure that all four cells were identical, their charge-discharge curves varied significantly from one another as seen in Figure 3.4. Such large difference in the voltage profiles cannot be attributed to inconsistencies in cell assembly or non-uniformity of LTO electrode. The curves indicate towards an increase in cell internal resistance. It is a well-studied phenomenon that LIBs show increasing internal resistance with decreasing porosity of the electrodes. [49]

Therefore, it is possible that the 270 nm sized AKP30 alumina particles are small enough to infiltrate into the pores of the LTO electrode and reduce its porosity. Since this infiltration is unintentional and occurring irregularly, it may be more severe in some cells than others, leading to different charge-discharge curve characteristics.

This theory is further supported by the fact that the LTO active material particles are approximately 2 μm in size. Therefore, the pore size can be approximated to at least 1.5 μm or smaller. A SEM image of the bare LTO electrode was also taken to verify the LTO particle size as seen in Figure 4.5.

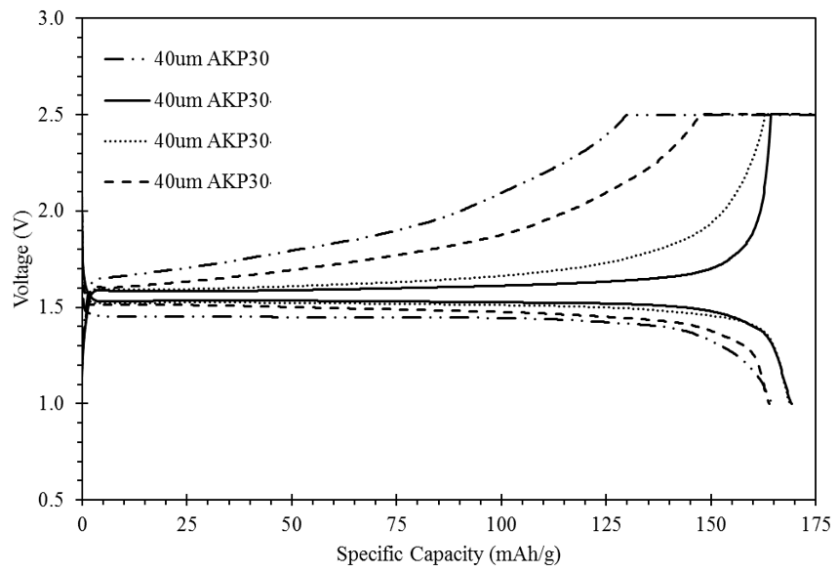


Figure 3.4. Charge-Discharge curves for LTO/Li half cells with 40 μm thick AKP30 separator at 0.2C rate.

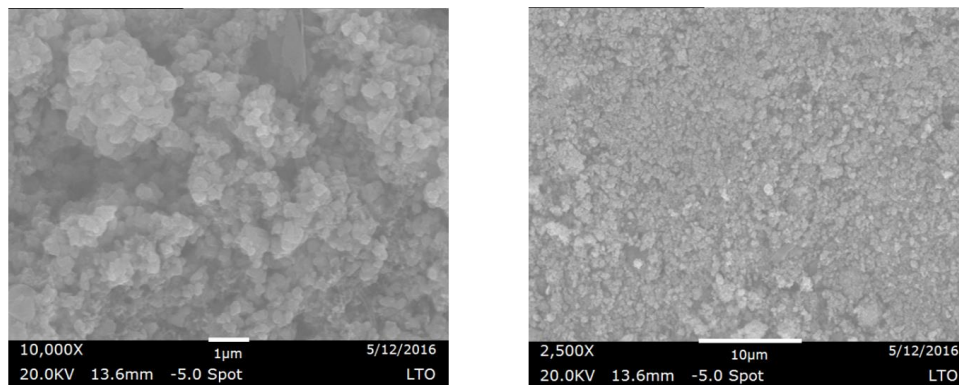


Figure 3.5. SEM image of Lithium Titanium Oxide (LTO) electrode at 10000x (left) and 2500x (right).

This explanation would be further supported if the charge discharge curves of multiple LTO/Li half-cells with A17SG coated alumina separator would be similar to each other. This is because most of the particles in the powder are $\sim 5 \mu\text{m}$ in size. Alumina particles of this large size would find it difficult to infiltrate into the LTO electrode, hence not affecting its porosity much. From the charge-discharge curves in Figure 3.6, it can be seen that three LTO/Li half cells with A17SG coated alumina separator show quite similar performance to each other. These three cells were also assembled identically. The slight variation in the curves can be explained by the small fraction of nano-sized alumina particles in A17SG powder that might have infiltrated into the electrode. The variations are in that region of voltage profile where concentration overpotential dominates the curve, which agrees with the fact that reduced porosity will affect bulk diffusion of lithium ions. But overall, the cells with coated A17SG separator show quite similar and reproducible results.

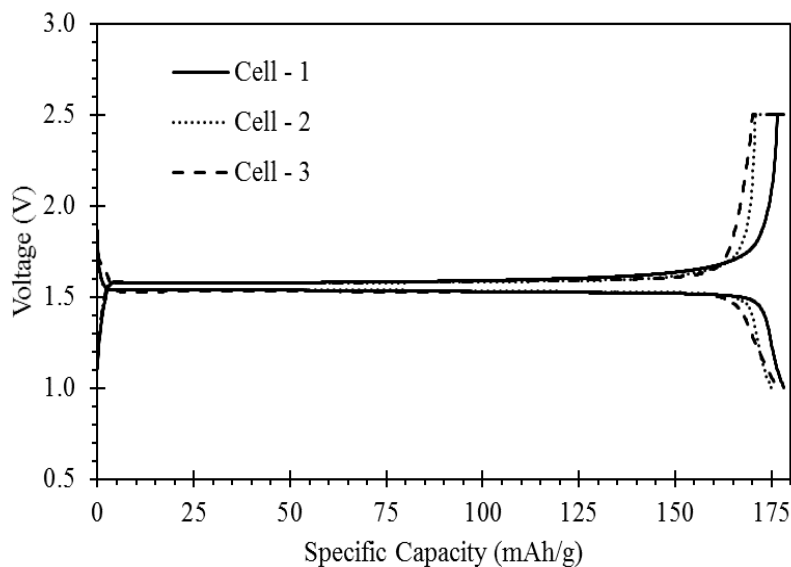


Figure 3.6. Charge-discharge curves of three LTO/Li half cells with 40 μm thick A17SG separator at 0.2C rate.

3.6 Conclusions

Alumina is a cheap inorganic material that can find application in preparing separators for safe LIBs. Alumina in its powdered form has several advantages like ease in processing, large surface area to improve wettability and good electrolyte retention. These properties reduce the MacMullin number of coated alumina separators compared to PP separator. Hence, the same thickness a coated alumina separator will add lesser internal resistance to a cell than commercial PP separator.

Several different types of alumina powders with different particle size distributions were formed into slurry and observed for consistency. It was found that very large particles with size $>20 \mu\text{m}$ tend to settle down and form unstable slurries. Powders with particle size less than $1 \mu\text{m}$ can form slurry only if the powder itself is free from

aggregates. And finally powders with particle size between 1 μm and 20 μm easily form good quality slurry free from aggregates as they break down easily.

The next study focused on the effect of particle size on coating quality. Powders with particles size larger than 10 μm are unable to form separator with 40 μm thickness as the particles size is too big compared to the blade gap needed for the two step coating process. This sets the upper limit to 10 μm for alumina powder particle size.

The final study observed the effect of alumina particle size on cell performance. Alumina powders with particle size smaller than the pore size of the electrode tend to infiltrate into the electrode and reduced its porosity. This results in inconsistent charge-discharge characteristics and increased resistance in the cells. Therefore, this further narrows down the particle size range to 5-10 μm for the alumina powder as these particles will not be able to infiltrate much into the electrode and give good reproducible cell performance.

CHAPTER 4

HIGH TEMPERATURE STUDY ON NMC/LTO FULL CELL

4.1 Introduction

The feasibility of coated alumina separator has been established using half-cells as seen in Chapter 2. However, the eventual application of this separator would be in full cells to improve their safety characteristics. Therefore, the aim of this chapter would be to test this separator in a full cell and study the improvement in safety at high temperatures.

With the advancement of technology in portable electronics and electric vehicles, LIBs with higher energy density, higher power density, safety and cycling performance have become the need of the hour. [33] Most efforts made in this direction are focused on developing new electrode materials.

Lithium Cobalt Oxide (LCO) is one of the most widely used cathode materials in LIBs. The trigonal structure of LCO allows lithiation and delithiation to occur. However, there are several limitations to LCO, mainly the high cost and toxicity associated with cobalt. In addition, LiCoO_2 is not stable and gets degraded when overcharged as the cobalt gets dissolved in the electrolyte when the electrode is delithiated during charging. This leads to reduced capacity with every subsequent cycle. Another promising cathode material is Lithium Manganese Oxide (LMO) due to its lower cost and improved safety. But this material has a lower capacity and also faces a problem of Mn ion dissolution in the electrolyte. An entirely different family of cathode materials are the phosphates with olivine crystal structure. Lithium Iron Phosphate (LFP) is the most popular due to its flat voltage profile and safety, but exhibit low capacity. [34]

Recently, there has been a great deal of interest in a new cathode, Lithium Nickel Manganese Cobalt Oxide (NMC). The three transition metals are maintained at equal weight ratios to form $\text{LiNi}_{1/3}\text{Mn}_{1/3}\text{Co}_{1/3}\text{O}_2$. NMC attracts lots of attention for its lower cost, less toxicity and higher capacity, which makes it superior to the commercial LCO. NMC has been reported to have a capacity as high as 200 mAh/g while maintaining good cycle performance between 2.8 and 4.6V. [33, 35]

On the other hand, anode materials have also received great attention. Graphite is the most commonly used anode by far. This is mainly because it has a flat and low working potential against lithium. Also, it is low cost and has a good cycle life. However, six carbon atoms of graphite can intercalate only one Lithium ion between them, this translates roughly into a reversible capacity of only 372 mAh/g. The low diffusion rate of lithium ions into the bulk of the electrode also results in low power density.

Ideally, Lithium metal itself would be the best anode material with 3860 mAh/g of specific capacity, but safety issues prevent the realization of this as an anode. The lithium dendrites still remain a major concern as they short circuit the cell. [36] Lithium Titanium Oxide (LTO) has a theoretical capacity of 175 mAh/g in the voltage range of 1.0-2.5V. It is gaining popularity due to its “zero-strain” property, which means that no changes occur in its lattice parameters upon insertion of lithium ions. This makes it an ideal candidate for batteries that require long life cycling. LTO also generates less heat than graphite when fully lithiated. LTO also exhibits better rate capability than graphite due to better lithium ion solvation and lack of SEI layer formation. LTO also rarely forms lithium dendrites because of its high redox potential of 1.55 V against Li. This is much

higher than other anode materials. [37] Therefore, LIBs with NMC as cathode and LTO as anode have become a highly attractive battery system, especially for electric vehicles.

However, safety is still a concern for most lithium ion batteries. In the event of inefficient heat dissipation from the battery, cell temperatures can rise to 130-150 °C. This causes uncontrolled exothermic reactions to set in between the electrodes and the electrolyte, which further increases the cell temperature and the cell is said to have entered thermal runaway. Thermal runaway is also caused by overcharging, high pulse power and mechanical causes like crushing and rupturing etc. During thermal runaway, several changes occur in the cell: (i) thermal decomposition of the electrolyte, (ii) electrolyte gets reduced by the anode, (iii) oxidation of electrolyte by the cathode, (iv) thermal decomposition of both the electrodes, (v) melting of the separator which leads to short circuit of the cell. [38]

Inorganic separators for LIBs are developed as a solution to the separator melting problem. Most commercial LIBs use polymer separators. These separators are usually porous thin films of polyolefins like Polyethylene or Polypropylene. These polymers not only have low melting points (130 – 150 °C), but before melting, they begin to shrink much earlier (80 – 100 °C) as seen in Figure 10. This shrinkage and subsequent melting worsen the cell conditions which is already under thermal runaway. A large short circuit is developed after separator deformation which causes a large current to flow through the cell and the battery pack can catch fire or explode. [3]

Since inorganic materials are ceramic in nature, they have very high melting points (>1000 °C). The temperature achieved during a thermal runaway is far lesser than this (130 – 150 °C), hence a separator made of such a material is expected to be

dimensionally and mechanically stable at such temperatures. Several inorganic separators have been reported [14-20] that exhibit dimensional stability when exposed to high temperatures. They withstand any shrinkage stresses, which will prove to be advantageous as the electrodes will not be able to come in contact with each other. This can prevent the flow of large short circuit current and the battery from catching fire or exploding.

We have developed an inorganic separator from α -Al₂O₃ powder which is coated directly on the electrode. The separator contains a small amount of polyvinyl alcohol (PVA) binder at just 0.4 wt%. Since the separator is coated directly on the electrode, it is supported by the electrode. Half cells were assembled in which LTO electrode was coated with this inorganic separator and lithium foil was used as the anode. The cell showed improvement in wettability and comparable electrochemical performance to that of half cells with polyolefin separators. Under extreme temperatures, the cells with the inorganic separator showed improvement in cycling performance.

Previously, a study was also conducted in which the shrinkage of the inorganic separator was observed with increasing temperature and compared to PP and PE separators over a temperature range of 25 – 180 °C. The coated alumina separator showed exceptional dimensional stability over the entire temperature range with no shrinkage. On the other hand, the PP and PE separators started to shrink around 80°C. The PE separator completely melted at around 130 °C while the PP separator melted at around 170 °C.

Even though the shrinkage test gives a good indication of the thermal stability of a separator inside a cell, it is more convincing if this advantage is demonstrated in a cell.

Since the eventual application of the coated alumina separator will be in a full cell, we decided to assemble NMC/LTO full cells with coated alumina separator. In the first case, NMC/LTO cell was assembled in which the alumina separator was coated on LTO electrode while in the second case, the alumina separator was coated on NMC electrode. This experiment would shed light on whether it makes any difference if the anode is coated or the cathode. The NMC/LTO cell with coated alumina separator was then exposed to stepwise increasing temperatures from 25 °C to 200 °C and was simultaneously monitored for any short circuiting. For comparison purpose, NMC/LTO full cells with PP and PE separators were also assembled and tested in the same fashion. This kind of a demonstration of improved safety of LIB will prove to be highly beneficial in the development of safe LIBs.

4.2 Experiment

4.2.1 Preparation of separator

The thin porous α -Al₂O₃ separator was coated directly on lithium titanium oxide (Li₄Ti₅O₁₂) and lithium nickel manganese cobalt oxide (LiNi_{1/3}Mn_{1/3}Co_{1/3}O₂) (NMC) electrodes by the same two-step blade coating process as described in Chapter 2.

4.2.2 Cell assembly

The cells assembled for this study were CR2032 type coin cells (X2 Labwares, Singapore). Two kinds of NMC/LTO full cells with the coated alumina separator were assembled. One with the NMC cathode which was coated with alumina, and the other in which LTO anode was coated with alumina separator. The coin cells were assembled in an argon-filled glove box (Innovative Technology Inc, Amesbury, MA), in which oxygen and moisture content were kept below 0.5 ppm.

A typical full cell was assembled by placing a 16 mm diameter alumina-coated LTO or NMC disk into the CR2032 casing. The separator was then filled with 80 μ L of the electrolyte and then covered with a 14 mm diameter of the counter electrode. Spacers and spring completed the cell which was then sealed using a coin cell crimper (MSK-110) (MTI, Richmond, CA) with a pressure of 650 psi. The cell specific capacity was calculated based on the active material mass in the smaller of limiting electrode. Similarly, NMC/LTO full cells with PP and PE separator were also prepared using 16 mm diameter LTO as anode and 14 mm diameter NMC as cathode for comparison. The PE and PP separator were 16 mm in diameter and were also filled with 80 μ L of the electrolyte.

4.2.3 Electrochemical characterization

The charge-discharge cycling characteristics of the cells was tested using NEWARE battery testing system (BTS3000) (Neware Co, Shenzhen, China). The cut-off voltage window setting for the NMC/LTO full cells was 0.5-3.5 V. All the cells were cycled using the CC-CV (Constant Current – Constant Voltage) charging regime. The cells were cycled at a medium current of 0.3 mA.

For high temperature testing, the full cells were inserted into an oven (temperature range: -40 to 150 $^{\circ}$ C) (WD4005, Shanghai Jianheng Instruments, Shanghai, China) while they were connected to the PARSTAT 2263 EIS station (Princeton Applied Research, Oak Ridge, TN) at 100% SOC. The temperature in the oven was increased by 10 $^{\circ}$ C after every 1 hour in the temperature range of 20 $^{\circ}$ C to 130 $^{\circ}$ C. At every temperature, the cell impedance was noted down by using the EIS station in the galvanostatic EIS mode

(GEIS) at a constant frequency of 1 kHz and 200 μ A rms AC amplitude. Beyond 130°C and up to 200°C, the cell impedance values were noted down more frequently.

4.3 Results and Discussion

The previous study in Chapter 2 focused on half-cells with coated alumina as the separator. LTO/Li and NMC/Li half cells with coated alumina separator showed good cycling performance. Based on these encouraging results, the next step was to assemble LTO/NMC full cells with coated alumina separator. This is important from scale up and commercialization point of view. Two NMC/LTO full cells were assembled. The first cell had the NMC cathode coated with alumina separator of 60 μ m thickness and bare LTO was the anode. The charge-discharge curve is shown in Figure 4.1. The second cell had the LTO anode coated with alumina separator 60 μ m thickness and bare NMC as the cathode. Its charge-discharge curve is shown in Figure 4.2. In both the cells, one electrode was kept larger than the other (i.e. the coated electrode was 16 mm in diameter while the uncoated electrode was 14 mm in diameter). This was done to avoid any short circuit from the cracks on the edge of the coated electrode that form when the disk cutter is used.

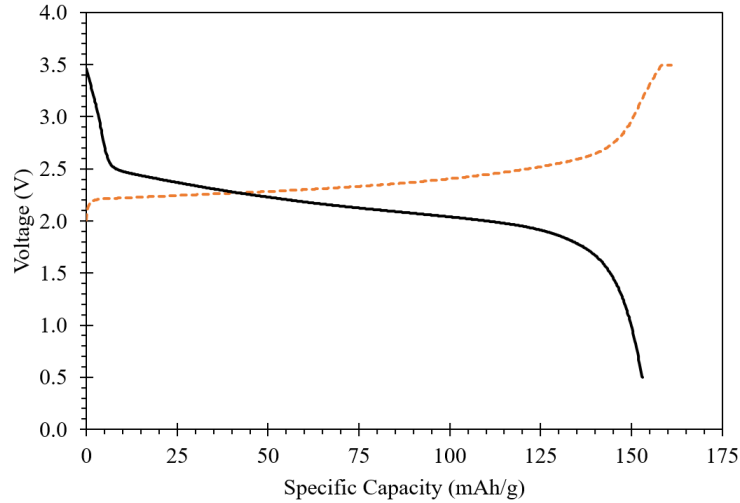


Figure 4.1. Charge-discharge curve of a full cell with NMC cathode coated with 60 μm thick alumina separator. A bare piece of LTO is the anode. The cell was cycled at 0.3 mA.

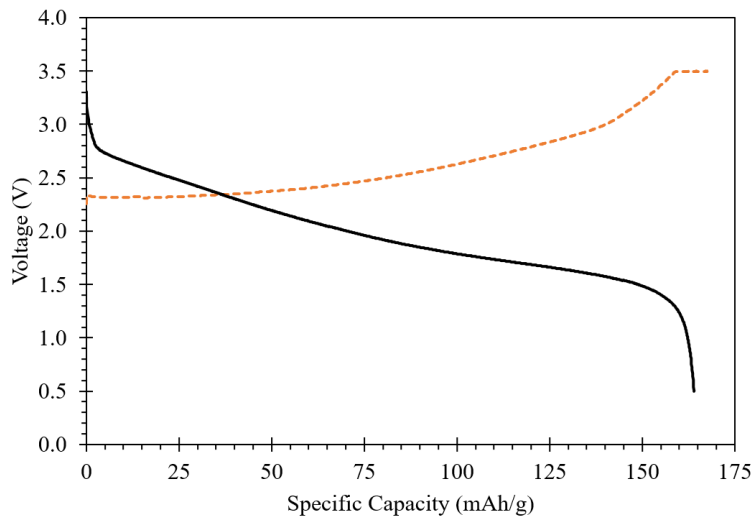


Figure 4.2. Charge-discharge curve of a full cell with LTO anode coated with 60 μm thick alumina separator. A bare piece of NMC is the cathode. The cell was cycled at 0.3 mA.

From Figure 4.1 and 4.2, we can see that both the full cells are able to cycle in the voltage range of 0.5 – 3.5 V. There is no short circuit or cracking/delamination of the

alumina separator. The charge-discharge curves in Figure 4.2 indicate a slightly higher internal resistance than the cell in Figure 4.1. It is likely a discrepancy that occurred during cell assembly. The motive of this study was only to see the feasibility of the NMC/alumina/LTO electrochemical system and that either of the electrodes can be coated as per the manufacturer's preference.

One of the main advantages of the coated alumina separator is its thermal stability. Thermal shrinkage study from the previous chapter showed that the alumina separator does not shrink or melt even up to 180 °C while the polymer PP and PE separators shrank and melted. Since the shrinkage of the separator leaves portions of the electrode exposed, it was expected that this would lead to a short-circuit in a cell. To verify this, three NMC/LTO full cells were assembled with the coated-alumina, PE and PP separators. The charge and discharge curves of NMC/LTO cells with PP and PE cells are shown in Figure 4.3 and 4.4 respectively for reference.

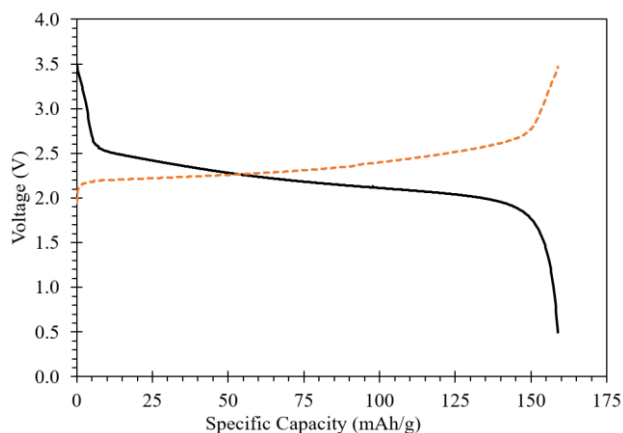


Figure 4.3. Charge-discharge curve of a full cell with NMC cathode and LTO anode. The separator used is the Celgard PP2500 (Polypropylene). The cell was cycled at 0.3 mA.

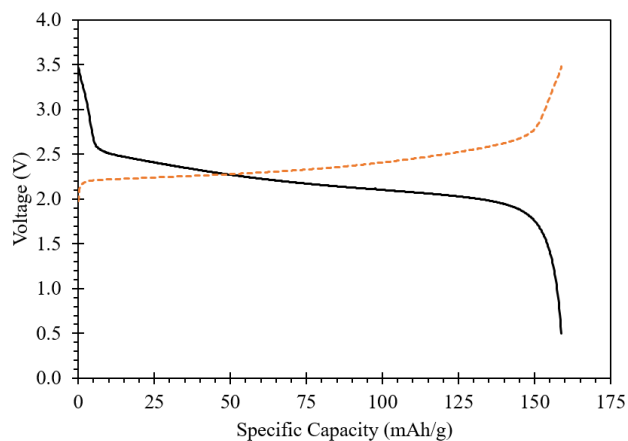


Figure 4.4. Charge-discharge curve of a full cell with NMC cathode and LTO anode. The separator used is the Entek Teklon Gold LP (Polyethylene). The cell was cycled at 0.3 mA.

The cells were then connected to the EIS station for cell impedance measurement at a constant frequency of 1 kHz using the GEIS setting. Simultaneously, the cells were kept inserted in an oven which controlled the ambient temperature in the same stepwise manner as the shrinkage test. At every temperature point, the cells were allowed to attain steady state for at least 15 minutes. As seen in Figure 4.5, data points were recorded more frequently beyond 120°C as the thermal effects were expected to be more pronounced in this temperature range.

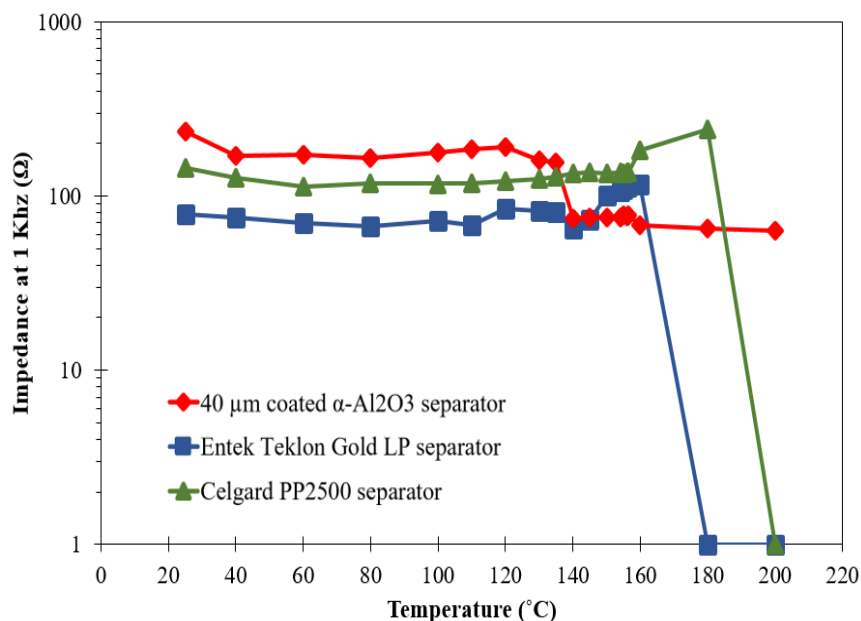


Figure 4.5: Cell impedance as a function of increasing temperature measured for NMC/LTO full cells with coated-alumina, PE and PP separators at 1 kHz galvanostatic EIS frequency.

The characteristic increase in the impedance for the polymeric separators is due to their shutdown property. [39] This begins to occur at around 140°C and 160°C for PE and PP separators respectively. As the temperature continues to increase, the cell impedance suddenly drops to zero at around 180°C and 200°C for PE and PP separators, indicating that a short-circuit has occurred. On the other hand, the cell with the coated-alumina separator does not short-circuit in this entire temperature range. Its dimensional integrity maintained the electronic insulation between the electrodes. The fluctuations in the impedance values can be attributed to the electrolyte instability at such high temperatures and can be neglected since the aim of this study was only to detect short-circuit.

4.4 Conclusions

Recently developed electrodes, NMC as cathode and LTO as anode were used to assemble full cells. The coated alumina separator was found to be suitable for application in LIBs since the cells were able to cycle satisfactorily. The cell performance is independent of which electrode is coated. Thus, the manufacturer has the flexibility to coat either the anode or cathode. The cell with coated alumina separator was able prevent a short circuit even at a temperature as high as 200 °C, whereas cells with PP and PE separators short circuited due to melting. This is a significant result as NMC/LTO batteries with coated alumina separator can be safer and less likely to short circuit during thermal runaway.

CHAPTER 5

SUMMARY AND RECOMMENDATIONS

5.1 Summary

This thesis presented an inorganic separator for lithium ion batteries made from α - Al_2O_3 (alumina) powder. The separator was prepared from a slurry of alumina powder, PVA binder and DI water which was blade coated directly on LIB electrodes such as LTO and NMC. In order to reduce the thickness of the separator down to 40 μm , a two-step blade coating procedure was developed. The first coat of the slurry was intended to make the surface of the electrode rough. This roughness produces frictional force that opposes the shear force from the motion of the blade. As a result, the slurry was prevented from sliding off the electrode and a good quality coat was obtained. Both LTO and NMC electrodes were coated with the alumina slurry and no noticeable difference was observed in the separator quality and performance. Therefore, NMC/LTO full cells were also assembled and tested in which either of the electrodes were coated. The cells were able to cycle within the specified voltage window with satisfactory performance.

Due to the inherent property of alumina powder of having high hydrophilicity, the coated alumina separator was able to get completely wet easily by different types of electrolytes, while commercial PP separator was found to be selective in getting wet with only certain electrolytes. Half-cells assembled with coated alumina separator showed electrochemical performance similar to that of half-cells with commercial PP and PE separators. During charge-discharge test, rate capability test, long-term cycling and electrochemical impedance spectroscopy, the coated alumina separator exhibited comparable performance to PP separator in spite of being almost twice as thick.

However, under extreme temperatures (-30 °C to +60 °C), higher electrolyte retention and scavenging properties allowed the cells with coated alumina separator to show better cycling performance than the cell with PP separator.

A closer look was taken at the effect of alumina powder particle size on slurry consistency, coating quality and cell performance. It was found that alumina powder with particle size 5-10 μm size produces slurry with good consistency (free from aggregates), good coating quality and consistent cell performance. Particles of this size are unable to infiltrate into the electrode substrate during preparation. This prevents any alterations to the electrode morphology such as porosity.

Lastly, one of the main advantages of alumina powder is its resistance to temperature effects and its exceptional thermal stability. Due to its very high melting point, separator made with alumina powder did not shrink or melt up to 200 °C. On the other hand, polymer separators like PP and PE first shrank and eventually melted. This dimensional stability of coated alumina separator could prove to be advantageous during a thermal runaway when cell temperatures increase rapidly. In this situation, the alumina separator would prevent the electrodes from coming in contact and short circuit can be prevented. This was proven experimentally on three NMC/LTO full cells with coated alumina, PP and PE separators respectively. At very high temperatures (>160 °C), cells with PP and PE separator short circuited as the separators melted. However, the cell with coated alumina separator was able to prevent a short circuit. This result can be helpful in development of safe batteries which do not catch fire or explode during thermal runaway.

Hence, several aspects of coated alumina separator have been studied and the separator is established as a promising and robust technology for safe LIBs.

5.2 Recommendations

Based on the experiments and results discussed in this thesis, following are a few recommendations for future work:

1. The advantage of using the coated alumina separator in preventing short circuit at high temperatures will be more pronounced in pouch cells than in coin cells. Due to the small area of coin cells, the shrinkage of the polymer separator was not enough to cause the cell to short circuit. In a large battery, shrinkage of the separator would be sufficient in exposing the electrodes to each other. However, in the coin cells, only when the polymer separators melted did the cell short circuit. Hence, it would be interesting to see this study being repeated in cells with large separator/electrode surface area.
2. Thermal stability of coated alumina separator can be further explored with nail penetration test. A short circuit induced by a nail piercing into a cell with the alumina separator would not be able to shrink and melt the separator, which is usually the case with the polymer separators.
3. Even though a major fraction of A17SG powder is consisted of alumina particles of $\sim 5 \mu\text{m}$ size, there are still some sub-micron size alumina particles that could be infiltrating into the electrodes during the synthesis of coated alumina separator. Hence, it would be preferable to use a unimodal alumina powder with particle size between 5-10 μm if available.
4. The viscosity of the alumina slurry should be quantified so that a standard slurry can be prepared even if other types of inorganic powders are used.

REFERENCES

- [1] J.M. Tarascon and M. Armand, *Nature*, **414**, 359-367 (2001).
- [2] H. Lee, M. Yanilaz, O. Topracki, K. Fu and X. Zhang, *Energy Environ. Sci.*, **7**, 3857-3886 (2014).
- [3] Q. Wang, P. Ping, X. Zhao, G. Chu, J. Sun and C. Chen, *J. Power Sources*, **208**, 210–224 (2012).
- [4] D. Lisbona and T. Snee, *Process Safety Environ. Protection*, **89**, 434–442 (2011).
- [5] S.S. Zhang, *J. Power Sources*, **164**, 351–364 (2007).
- [6] X. Huang, *J. Solid State Electrochem.*, **15**, 649–662 (2011).
- [7] M.H. Ryou, Y. M. Lee, J.K. Park and J. W. Choi, *Adv. Mater.*, **23**, 3066–3070 (2011).
- [8] C. L. Eggen, P. M. McAfee, Y. Jin and Y.S. Lin, *Thin Solid Films*, **591**, 111–118 (2015).
- [9] D. Goeriot-Launay, G. Brayet and F. Thevenot, *J. Mat. Sci. Letters*, **5** (9), 940-942 (1986).
- [10] C. Shi, P. Zhang, L. Chen, P. Yang and J. Zhao, *J. Power Sources*, **270**, 547-553 (2014).
- [11] J. Choi, S. H. Kim and D. Kim, *J. Power Sources*, **195**, 6192–6196 (2010).
- [12] S. S. Zhang, K. Xu and T. R. Jow, *J. Solid State Electrochem.*, **7**, 492–496 (2003).
- [13] S.S. Zhang, K. Xu and T.R. Jow, *J. Power Sources*, **140**, 361–364 (2005).
- [14] H. Xiang, J. Chen, Z. Li and H. Wang, *J. Power Sources*, **196**, 8651– 8655 (2011).
- [15] J. Chen, S. Wang, D. Cai and H. Wang, *J. Membr. Sci.*, **449**, 169–175 (2014).
- [16] J. Chen, S. Wang, L. Ding, Y. Jiang and H. Wang, *J. Membr. Sci.*, **461**, 22–27 (2014).
- [17] M. He, X. Zhang, K. Jiang, J. Wang and Y. Wang, *ACS Appl. Mater. Interf.*, **7**, 738-742 (2015).
- [18] M. Raja, N. Angulakshmi, S. Thomas, T. Prem Kumar and A. Manuel Stephan, *J. Membr. Sci.*, **471**, 103–109 (2014).

- [19] J. Holtmann, M. Schäfer, A. Niemöller, M. Winter, A. Lex-Balducci and S. Obeidi, *J. Appl. Electrochem.* **46**, 69–76 (2016).
- [20] M. Kim, Y. Nho and J. H. Park, *J. Solid State Electrochem.*, **14**, 769–773 (2010).
- [21] K. Hamano, US Patent 5981107 A, Nov 9, (1999).
- [22] W. Mi, G. Sharma, X. Dong, Y. Jin and Y.S. Lin, *J. Power Sources*, **305**, 209 – 216 (2016).
- [23] I. Yamada, T. Abe, Y. Iriyama and Z. Ogumi, *Electrochem. Comm.*, **5**, 502–505 (2003).
- [24] J. Y. Kim and D. Y. Lim, *Energies*, **3**, 866-885 (2010).
- [25] H. Maleki and J. N. Howard, *J. of Power Sources*, **191**, 568–574 (2009).
- [26] R. Mahamud and C. Park, *J. Power Sources*, **196**, 5685–5696 (2011).
- [27] S.S. Zhang, K. Xu and T.R. Jow, *Electrochimica Acta*, **49**, 1057–1061 (2004).
- [28] Y.H. Liao, X.P. Li, C.H. Fu, R. Xu, L. Zhou, C.L. Tan, S.J. Hu and W.S. Li, *J. Power Sources*, **196**, 2115-2121 (2011).
- [29] N. Zhua, W. Liu, M. Xuea, Z. Xiea, D. Zhaoa, M. Zhang, Jitao Chen and T. Caoa, *Electrochimica Acta*, **55**, 5813–5818 (2010).
- [30] J. Zhang, L. Yue, Q. Kong, Z. Liu, X. Zhou, C. Zhang, Q. Xu, B. Zhang, G. Ding, B. Qin, Y. Duan, Q. Wang, J. Yao, G. Cui and L. Chen, *Scientific Reports*, **4**, 3935 (2014).
- [31] W. Xu, Z. Deng and P. Bolomey, US Patent 8273484 B2.
- [32] J. L. Tebbe, A. M. Holder and C. B. Musgrave, *Appl. Mater. Interfaces*, **7**, 24265–24278 (2015).
- [33] Y. Han, Z. Zhang, L. Zhang, J. Peng, M. Fu, C. Srinivasakannan and J. Du, *Trans. Nonferrous Met. Soc. China*, **23**, 2971–2976 (2013).
- [34] J. W. Fergus, *J. of Power Sources*, **195**, 939–954 (2010).
- [35] J. Choi and A. Manthiram, *J. Electrochemical and Solid State Lett. A*, **7(10)**, 365–368 (2004).

- [36] S. Goriparti, E. Miele, F. De Angelis, E. Di Fabrizio, R. P. Zaccaria, C. Capiglia, *J. of Power Sources*, **257**, 421-443 (2014).
- [37] K. Wu, J. Yang, Y. Zhang, C. Wang and D. Wang, *J. Appl. Electrochem.*, **42**, 989–995 (2012).
- [38] P.G. Balakrishnan, R. Ramesh and T. Prem Kumar, *J. of Power Sources*, **155**, 401–414 (2006).
- [39] G. Venugopal, J. Moore, J. Howard and S. Pendalwar, *J. Power Sources*, **77**, 34–41 (1999).
- [40] D. Takemura, S. Aihara, K. Hamano, M. Kise, T. Nishimura, H. Urushibata and H. Yoshiyasu, *J. of Power Sources*, **146**, 779–783 (2005).
- [41] K. M. Abraham, *Electrochimica Acta*, **38 (9)**, 1233-1248 (1993).
- [42] R. Hadar, D. Golodnitsky, H. Mazor, T. Ripenbein, G. Ardel, Z. Barkay, A. Gladkikh, and E. Peled, *J. Phy. Chem*, (2012).
- [43] M. J. Martínez, S. Shimpalee and J. W. Van Zee, *J. of Electrochem. Soc.*, **156 (1)** B80-B85 (2009).
- [44] P. Arora and Z. Zhang, *Chem. Rev.*, **104**, 4419–4462 (2004).
- [45] D. Djian, F. Alloin, S. Martinet, H. Lignier and J.Y. Sanchez, *J. of Power Sources*, **172**, 416–421 (2007).
- [46] K. K. Patel, J. M. Paulsen and J. Desilvestro, *J. of Power Sources*, **122**, 144–152 (2003).
- [47] I. V. Thorat, D. E. Stephenson, N. A. Zachariasa, K. Zaghbib, John N. Harb and D. R. Wheeler, *J. of Power Sources*, **188**, 592–600 (2009).
- [48] M. Kirchhöfer, J. von Zamory, E. Paillard and S. Passerini, *Int. J. Mol. Sci.*, **15**, 14868-14890 (2014).
- [49] H. Buqa, D. Goers, M. Holzapfel, M. E. Spahr and P. Novak, *J. of Electrochem. Soc.*, **152 (2)**, A474-A481 (2005).

APPENDIX A

PROCEDURES TO ASSEMBLE HALF-CELLS AND FULL CELLS

A1. Operation of Glovebox

1. Refill the small antechamber with working gas to remove the vacuum. This should allow the door to open.
2. Load samples into the small antechamber.
3. Turn on vacuum pump and alternately evacuate and refill the small antechamber at least 3 times.
4. Open the door of the small antechamber from the inside of the glovebox to obtain sample. Care must be taken that nitrile gloves are worn under as well as over the glovebox gloves.
5. After assembling the cell, load the samples back into the small antechamber and firmly close the door from the inside.
6. Gently remove your hands from the gloves and open the outside door of the small antechamber to obtain your sample.
7. Close the outside door firmly and turn on the vacuum pump to put the small antechamber back under vacuum.

A2. Assembly of Half-cell

1. Take the negative shell of CR2032 type coin cell cases.
2. Place the alumina-coated LTO or NMC electrode of 16 mm diameter in the negative shell.
3. Using a pipette, add 150 μL of electrolyte on the separator coating layer.
4. Cover the separator with a flattened piece of Lithium foil of diameter 15.5 mm.
5. Place two spacers on top of the lithium foil.
6. Place one spring on top of the spacers.

7. Enclose the cell with the positive shell of the CR2032 type coin cell cases
8. Crimp the cell using the crimping machine (MSK-110, MTI) using a pressure of 450 psig.
9. Clean the exterior of the cell for any excess electrolyte that comes out during crimping.

A3. Assembly of Full-cell

1. Take the negative shell of CR2032 type coin cell cases.
2. Place the alumina-coated LTO or NMC electrode of 16 mm diameter in the negative shell.
3. Using a pipette, add 150 μL of electrolyte on the separator coating layer.
4. Place the counter electrode of diameter 14 mm on top of the soaked separator.
5. Place two spacers on top of the counter electrode.
6. Place one spring on top of the spacers.
7. Enclose the cell with the positive shell of the CR2032 type coin cell cases
8. Crimp the cell using the crimping machine (MSK-110, MTI) using a pressure of 600 psig.
9. Clean the exterior of the cell for any excess electrolyte that comes out during crimping.

APPENDIX B
CYCLE TESTING OF CELLS

1. Mount the cells onto the NEWARE BTS3000 battery tester by placing the cell between the jaws of the alligator clip. Ensure that the anode side of the coin cell is connected to the negative (black) wire and cathode side to the positive (red) wire.
2. Open the NEWARE software and right click on the particular cell testing channel's icon and select 'Startup'
3. Setup the cycling steps in the following order
 - (i) Rest cell for 24 hours
 - (ii) Rest cell for 1 minute
 - (iii) Discharge at Constant Current at 0.1 C-rate
 - (iv) Rest cell for 1 minute
 - (v) Charge at Constant Current – Constant Voltage (CCCV) at 0.1 C- rate. Set 'End Current' to 15% of charging current.
 - (vi) Rest cell for 1 minute
 - (vii) Let the cell cycle at 0.1C for two cycles. These are the formation cycles.
 - (viii) Rest cell for 1 minute
 - (ix) Discharge at Constant Current at desired C-rate
 - (x) Rest cell for 1 minute
 - (xi) Charge at Constant Current – Constant Voltage (CCCV) at desired C- rate. Set 'End Current' to 15% of charging current.
 - (xii) Rest cell for 1 minute
 - (xiii) Leave the cell for testing for desired number of cycles.
 - (xiv) Select 'End'.
4. After all the cycles are completed, dismount the cell from the alligator clips.

APPENDIX C

ELECTROCHEMICAL IMPEDANCE SPECTROSCOPY OF CELLS

1. Connect the Sense and Working terminals of PARSTAT 2263 EIS station to the positive jaw of the alligator clip, while the Counter-electrode and Reference terminals should be connected to the negative jaw of the alligator clip.
2. After a cell has rested for 24 hours, mount the cell onto the alligator clip with the working electrode (or cathode) side of the coin cell facing the positive jaw of the alligator clip.
3. In the PowerSuite software, go to Tools → Database Management → Create New Database → Create a .mdb file.
4. Now, go to Experiment → New → Browse → Select the file created in Step 3
5. Select PowerSine → Single Sine → Default SS
6. In Scan Definition, set start frequency to 100 KHz and end frequency to 10 mHz
7. Set points/decade to 5.
8. Choose logarithmic point spacing and set AC amplitude to 10 mV rms and DC potential to 0 V.
9. Click finish to obtain Nyquist plot.

APPENDIX D

PROCEDURE TO MEASURE POROSITY OF COATED ALUMINA SEPARATOR

1. Weigh a 16 mm diameter piece of LTO electrode.
2. After coating LTO with the alumina separator, cut out a 16 mm diameter sample and weigh it.
3. The difference of the weights in Step 2 and Step 1 is the weight of the porous alumina separator layer.
4. Divide the weight of the porous alumina separator layer by the density of alumina (3.95 g/cm^3) to obtain the volume of the dense separator.
5. The total volume of porous separator is then calculated from the area and measured thickness of the separator layer.
6. The difference between the volume of porous separator (Step 5) and dense separator (Step 4) gives the pore volume of the alumina separator.
7. Divide the pore volume (Step 6) with the total volume (Step 5) to obtain the porosity of the alumina separator.

APPENDIX E

DETERMINATION OF OHMIC RESISTANCE OF A SEPARATOR USING EIS

1. Soak the piece of separator for 24 hours in the 1M LiPF₆ in EC/DEC/DMC (1:1:1 v/v/v) electrolyte.
2. Polish and press two identical stainless steel disks of 16 mm diameter to make them very flat and smooth. When held against each other, there should be no visible space in between them.
3. Measure the resistance of these disks using EIS (PARSTAT 2263) between 100 kHz and 100 mHz frequency. The point where the Nyquist plot meets the x-axis is recorded as the blank ohmic resistance reading Ω_{ss} . It should be ensured that they are well aligned when held against each other.
4. Place the soaked separators in between the disks. Add extra electrolyte to ensure good wettability. Again obtain the ohmic resistance as described in step 3 using EIS. This is recorded as Ω_{sep+ss} .
5. The difference between Ω_{sep+ss} and Ω_{ss} is the ohmic resistance of the separator.
6. For coated-alumina separator, the only difference is that the alumina slurry is coated on pure aluminum foil. Because of this, the blank reading is obtained with the aluminum foil placed in the between the stainless steel disks.